Modelling, and Aggressive Robust Load-Frequency Control of Electric Power Systems (ver3.3 - 30Sep2019 18.59)

Leonidas Dritsas[†], Efstathios Kontouras[†††], Eleftherios Vlahakis[††], Ioannis Kitsios[†††], George Halikias[††] and Anthony Tzes[††††]

***Abstract*— This article is concerned with modelling, controllability analysis and the design of aggressive robust controllers for interconnected electric power systems. The load/frequency controller relies on a pole clustering scheme and provides the fastest transient response despite any disturbance load application. The inherent saturation constraints are handled by the combination of a controller gain minimization scheme and an anti-windup enhanced controller design which provides stability guarantees, while avoiding frequency and tie-line power oscillations. For this scheme, particular attention should be paid on the modeling aspects of the power system. It is shown that due to the positive semidefinite graph-connection Laplacian of the system, a reduction of the state vector is necessary. Simulation studies are offered to illustrate the effectiveness of the suggested scheme.**

I. Introduction

This article suggests a framework of linear modelling, analysis and state feedback control design for the Load Frequency Control (LFC) problem of a power system consisting of multiple interconnected areas. Although this control loop has been extensively analyzed in the past [1–3], it is still an area of active research [4–12, **?**–12, **?**–12, **?**–12], mainly because the control design objectives are now revisited from a different, more complex, perspective. Deregulation, distributed generation and microgrids, renewable energy sources, coupled to security issues in power systems seen as cyber-physical systems [5–8, 10, 12, 13], lead to the increasing need and interest for intelligent distributed control [4, 14–16], while accounting for saturation induced instabilities [17, 18].

Despite the extended published work on LFC, there are still open issues for the system controllability and input saturation.

In this work, the linearized model's controllability issues due to the interconnecting inductive tie–lines are exposed. At the same time, an aggressive controller design coupled with large power loads necessitate the employment of anti-windup controllers to account for any input saturation.

[†]The author is with the Department of Electrical & Electronic Engineering Educators, School of Pedagogical & Technological Education, ASPETE, Athens, Greece.

[††]The authors are with the Electrical & Computer Engineering, City University London, UK.

[†††]The authors are with the Electrical & Computer Engineering Department, University of Patras, Rio 26500, Greece.

[††††]The author is with the Electrical & Computer Engineering, New York University Abu Dhabi, Abu Dhabi, 129188, United Arab Emirates.

A. Relevant Literature Review

LFC has been covered in [1–3, 19–21]. A recent LFC survey [22] discusses classical, optimal, robust, adaptive, sliding mode, self-tuning, and soft-computing control techniques. Another survey [23] examines conventional and distribution generation power systems, and highlights various modeling configurations and control strategies to account for battery energy storage systems (BESS/SMES), FACTS devices, wind–diesel and PV systems. [24] provides emphasis to soft computing based optimization techniques and the interwining of LFC with Energy Storage System (ESS), HVDC-links, Distributed Generation, micro grids and load forecasting. The limitations of the classical LFC controllers in a deregulated electric generation environment are examined in [25].

A taxonomy of the LFC-strategies are offered in [26] along with suggested research directions.

Reference [27] is among the first research efforts concerning LMI–based solutions to the LFC problem including the case of time delays in the measurement path, whereas [28], by the same research team, offers an overview of Real-Time Control, Communication, and Computations for Large Power Systems.

Reference [29] presents an LMI–based linear H_∞ approach with prespecified circular pole constraint, "D-stability", on the closed-loop system matrix. The analysis and synthesis are purely linear and does not address the nonlinearities commonly involved in LFC, i.e. input saturation or generation rate constraints.

Reference [15] presents a robust decentralized controller based on mixed H_2/H_∞ control technique for the solution of Load Frequency Control (LFC). It is shown that, subject to a condition based on the structured singular value (μ), each local area load frequency controller can be designed independently so that stability of the overall closed loop system is guaranteed.

Reference [30] presents the LFC problem for a realistic power system with multi-source power generation, taking into account generation rate constraints (GRCs) for the thermal and hydro plants. Dynamic output feedback controllers are designed and their performance is compared with that of the full state feedback controller. Sensitivity analysis for parameter variations, especially on the droop gains, reveals that the proposed controller is quite robust.

Reference [16] presents an optimal decentralized control approach for damping of inter-area oscillations in power systems with a guaranteed level of damping. A heuristic

iterative LMI algorithm is proposed which allows simultaneous design of the control structure and the control gain. Regional pole-placement constraints are taken into account and a prescribed level of damping is guaranteed. The control structure and the control gain are designed by minimizing the number of required communication links and maximizing the closed-loop performance.

Reference [4] discusses distributed and adaptive secondary control for microgrids containing inverter-based DGs and balanced loads. The proposed distributed control structure obviates the "single point of failure" drawback of conventional centralized secondary control structure and improves the reliability of the microgrid secondary control. It is shown that for microgrids, decentralized controllers are more reliable than centralized LFC, since there is no communication among constituent inverters.

Reference [18] presents an H_∞ Load Frequency Controller Design for Multi-Area Power System enhanced with an Anti-Windup scheme that handles Generation Rate Constraints.

B. The objectives and the achievements of this research effort

- This research work proposes a framework of linear modelling, controllability analysis and linear control design for a realistic version of the Load Frequency Control (LFC) problem for electric power systems consisting of multiple power areas interconnected via power tie lines.
- The objectives and contributions of this research work are twofold and thus the paper naturally consists of two parts: in the first part modelling and controllability issues are raised and solved in a way that, to the best of the authors' knowledge, has never been published before. The main contribution is the proof that when modelling is based on the full state vector, no matter what level of model complexity is used, state controllability is always lost due to the inherent positive semidefiniteness of the Graph Laplacian reflecting the tie–line interconnections. The loss of controllability gives rise to a non minimal state space representation with one uncontrollable pole at the origin. Accordingly it is shown that it is always possible to systematically "single out" and discard the redundant state variable acquiring a controllable reduced state model which can then be used without "loss of information" for feedback control design.
- the proposed linear control framework is a "baseline" static state feedback controller incorporating integral action so that the disturbance rejection objective is satisfied. The control design is based on well-established LMI–based H_∞ control methodologies enhanced with "pole clustering" constraints reflecting performance specifications. The controller is tuned according to the specifications set for the power system to be controlled, the nominal (expected) loads and various degrees of control action aggressiveness expressed via the designer's choice of pole clustering region i.e. the minimum decay–rate and damped angular frequency of the closed–loop system.
- In the second part, input saturation is added to the previous linear models in order to investigate its impact on performance. The main difficulty arising when (some kind of inevitable) input saturation is taken into account, is that the model becomes a multivariable nonlinear one, whose performance depends on the amplitude of the disturbances acting on it, making difficult to accurately predict and minimize the ensuing performance deterioration usually manifested as violent frequency and tie-line power oscillations unless the saturators are somehow embedded in the analysis and synthesis procedure.
- The controllable reduced state models, achieved systematically in the first part of this work, are used to investigate the interaction of standard linear control designs of increasing aggressiveness with input saturation. It is shown that even in the simplest possible non–trivial example of two interconnected power areas, the combination of an aggressive control design choice and power loads larger than the nominal ones (for which the controller was tuned), the frequencies and tie-line power manifest violent oscillations. The depicted performance deterioration when input saturation is taken into account is a clear indication of the danger ensuing when a "purely linear mentality" is followed and/or when the inevitable ever present nonlinearities are neglected.
- Two "linear remedies" are proposed as a solution to the performance deterioration problem: the first one is minimization of the 2-norm of the gains (attempting to keep actuation authority low) and the second one is an anti–windup scheme (with linear structure and LMI based synthesis) guaranteeing both closed-loop stability and the suppression of violent frequency oscillations (due to the "low-pass filtering" action of the AW compensator).
- It should be noted that our work concerns centralized LFC schemes concerning the (more or less) conventional power systems where the prime movers (steam/hydro turbines) and the synchronous generators with (usually) large inertias act as "smoothening filters" for the variations of the electric loads. This includes the important set of geographically remote (small steam/hydro power plants) operating either in islanded or grid-connected mode but, at this stage, does not cover all possible power generation alternatives. For example we are aware of the peculiarities associated with the presence of renewable sources in the ("P-f" and "Q-V") Control loops of Power Systems, peculiarities arising (i) from the presence of power electronics devices (e.g. Voltage Source Inverters/VSI) with nonlinear dynamics, (ii) low inertias, (iii) the stochastic nature of wind/sunlight power sources (windmills/photovoltaic respectively). Similar issues are also true for microgrids where, apart from the complications arising from the employed power electronics interfaces (VSIs), which have to be modelled separately, there is also a need of a more accurate electric machinery model (e.g. d-q analysis of alternators) [4, 20]. These issues are not

covered by the models used in our work.
- It should also be noted that in this work the use of the word "Robustness" signifies solely "bringing all frequency deviations and all tie–line power flows back to zero despite the presence of unknown loads" i.e. it reflects disturbance rejection, (no parametric uncertainty, no high frequency unmodelled dynamics).

C. Article's structure

The rest of the paper is divided in five sections. Section II presents in a systematic/structured way three commonly encountered generic open–loop models for the linearized dynamics of multiple interconnected power areas. Presentation starts by analyzing the signals and the system components of each model. Starting with subsection II-C, three different state space formulations are presented for the generic LFC problem for multiple interconnected power regions ("areas"). The important contribution here is that in all three offered formulations, state controllability is lost due to the presence of the positive semidefinite Graph Laplacian of the interconnecting tie–lines. Exploiting structural properties of the Laplacian, a similarity transformation is then presented in subsections II-D and II-E which reveals the redundant uncontrollable mode and recovers controllability via state vector reduction.

Section III shows how the generic modelling approaches and controllability loss/recovery can be exploited for Load Frequency Control design using standard, fully centralized LMI–based, H_∞ methodologies (for disturbance rejection) and pole clustering (for performance), combined with state augmentation in order to enforce integral action in the controller. Subsection III-C exemplify the previous generic modelling, controllability and control design results by presenting applications of these results on two areas, whereas subsection III-D repeats the example for a fully interconnected three area example.

Section IV introduces the second major contribution of this work, raising the issue of amplitude input saturation constraint on the control signal of each area. The perplexities when input saturation is taken into account and the problem of violent frequency oscillations in case of aggressive control objectives and larger–than–nominal loads are demonstrated via simulations, making clear the need for "extra action". Two enhancements on the baseline H_∞ controller of the previous sections are proposed, both of linear structure: Gain 2-norm minimization and an Anti–Windup (AW) compensation scheme, both designs expressed also via LMIs. Conclusions and directions for future research are offered in the last Section V.

Regarding notations, operator Δ denotes the deviation of a variable from its nominal value. $\mathbb{I}_N$ corresponds to the $N\times N$ identity matrix, $\mathbb{O}_N$ corresponds to the $N\times N$ zero matrix, $0_{N,P}$ is a zero matrix of appropriate dimensions, $1_N \in R^N$ is an "all–one" column vector while $0_N \in R^N$ is an "all–zero" column vector. The notation $\mathrm{diag}\,(X_1,\ldots,X_n)$ signifies a diagonal matrix with matrices $X_1,\ldots,X_N$ on the diagonal, while the expression $M>0$ (<0) implies that M is a positive (negative) definite matrix.

II. Linearized Models, state space formulation and control objectives for Load–Frequency Control

We consider the "Megawatt-Hertz" or Load–Frequency Control problem (henceforth LFC) for N interconnected power areas with each area modelled as a "aggregated" power plant whose power generation is affected by unknown loads (customer demand) and tie–lines connecting the area with other areas. The presentation is generic for N interconnected areas and the modelling part is inspired by previous research efforts presented in [1–3, 12].

Low dimension two and three–area examples are used for the clarification of the modelling concepts, the controllability issues and the notation used in this work, as well as benchmark problems for the sections presenting the application of standard control methodologies and simulation results.

A. The three different (open–loop) models encountered in the LFC literature

Three different area models of increasing complexity are commonly encountered in the LFC literature: the one–block model (only area dynamics), the two–block model (area and turbine/generator dynamics), the three–block model (area, turbine/generator and speed governor dynamics). For the sake of brevity we shall refer to them as Model-1, Model-2 and Model-3 respectively.

The single–block area model (Model-1), shown in Figure 1, is the simplest possible model using only the area dynamics transfer function (turbine and speed governor dynamics are ignored).

The two–block area model (Model-2) depicted in Figure 2 is comprised of the area dynamics and a turbine/generator block. Figure 5, exemplifies and clarifies the use of Model-2 for modelling of a benchmark two–area example.

The three–block area model (Model-3), depicted in Figure 3, apart from the area and the turbine/generator, includes also the linearized speed governor dynamics.

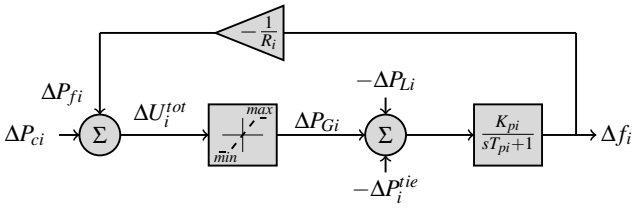

Fig. 1. One Block Area.

Two sets of signals are common to all three linearized power area models: The first set of signals is comprised of the components of the net power ΔP_i^{net} entering the area, i.e.(i) the power ΔP_{Gi} generated locally (by the lumped turbine/generators acting in the area), (ii) unknown loads ΔP_{Li} (local customer demand) and (iii) the net power inflow

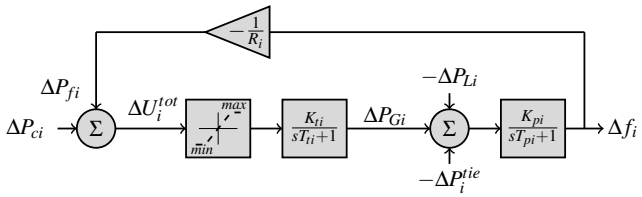

Fig. 2. Two-block model.

ΔP_i^{tie} borrowed via the tie–lines connecting each area with other neighboring areas.

The second set of signals concerns the components of the total control signal comprised of the primary frequency control action $(-1/R_i)\Delta f_i$ and the secondary control action $\Delta P_c i$ (a major part of the automatic generation control (AGC)).

B. The components of the linearized models - definitions and explanations

1) The speed governor block: The speed governor on each generating unit is the local actuator in each area, implementing the primary speed control function as well. All generating units contribute to the overall change in generation, irrespective of the location of the load change, using their speed governing. The speed governor senses and consequently compensates via the primary and secondary control loops the change in alternator speed (reflected directly into electrical frequency). In steam (or hydro) turbines for example, a hydraulic amplifier usually provides the necessary mechanical forces to position the main valve against the high steam (or hydro) pressure and the speed changer provides a steady-state power output setting for the turbine [2, 3]. If the inevitable steam valve saturation is ignored (or not triggered), the linearized speed governor dynamics is captured by a stable first order transfer function

$$\frac{K_{gi}}{sT_{gi}+1},\ i=1,2,\ldots,N$$

with the total control signal ΔU_i^{tot} as input and the output (state variable) ΔP_{vi} being the power command to the turbine/generator block. Taking into account the structure of $\Delta U_i^{tot} = \Delta P_{ci} - \frac{1}{R_i}\Delta f_i$ (to be explained in (8) below), the archetypal governor dynamics, used only in Model-3, is

$$\begin{aligned}\Delta\dot{P}_{vi} &= -\frac{1}{T_{gi}}\Delta P_{vi} + \frac{K_{gi}}{T_{gi}}\Delta U_i^{tot} \\ &= -\frac{1}{T_{gi}}\Delta P_{vi} + \frac{K_{gi}}{T_{gi}}\Delta P_{ci} - \frac{K_{gi}}{R_i T_{gi}}\Delta f_i \end{aligned} \quad (1)$$

More complicated speed governor models have been presented [3, 21] but the simple first order linear model used here is adequate for the presentation of the concepts and methodologies.

2) The turbine/generator block: The output (state variable) of the turbine/generator block (encountered in Model-2 and Model-3)

$$\frac{K_{ti}}{sT_{ti}+1},\ i=1,2,\ldots,N$$

is the deviation ΔP_{Gi} of the electrical power generated by the lumped alternators of each area from the desired steady–state value (both signals usually in MW). Moreover, ΔP_{Gi} is assumed to be equal to the mechanical power produced by the lumped (non reheat) turbines in each area. More complex (both linear and nonlinear) turbine models are available in the literature, but the one used here suffices for the purposes of this work.

The combined turbine/generator dynamics for the i-th area when a speed–governor block is included in the dynamics is

$$\Delta\dot{P}_{Gi} = -\frac{1}{T_{ti}}\Delta P_{Gi} + \frac{K_{ti}}{T_{ti}}\Delta P_{vi} \quad (2)$$

3) The control area block: The simplest model for the linearized (perturbed) dynamics of the i-th area is a stable first order plant. The input to each control area transfer function

$$\frac{K_{pi}}{sT_{pi}+1},\ i=1,2,\ldots,N$$

is the (perturbed) net power inflow $\Delta P_i^{net} = \Delta P_{Gi} - \Delta P_i^{tie} - \Delta P_{Li}$ fed into the area, whereas the output (state variable) is the frequency deviation Δf_i from the nominal value, common for each synchronous generator in the area. The static gain K_{pi} (Hz/MW) has to do with the load damping coefficient (the dependence of the load impedances on frequency) and the time constant T_{pi} has to do with the inertias of the rotating masses. The exact expressions for $K_{pi},\ T_{pi}$ will be given in the simulation section and will be related to the area parameters (see definitions (53) in following section).

The "archetypal" frequency dynamics in each area, common in all three models, is clearly

$$\begin{aligned}\dot{\Delta f_i} &= -\frac{1}{T_{pi}}\Delta f_i + \frac{K_{pi}}{T_{pi}}\Delta P_i^{net} \\ &= -\frac{1}{T_{pi}}\Delta f_i + \frac{K_{pi}}{T_{pi}}\Delta P_{Gi} - \frac{K_{pi}}{T_{pi}}\Delta P_i^{tie} - \frac{K_{pi}}{T_{pi}}\Delta P_{Li} \end{aligned} \quad (3)$$

4) The power loads acting as disturbances: The disturbance signals $\Delta P_{Li},\ i=1,\ldots,N$ correspond to unknown, piecewise constant and bounded power load deviations with known upper and lower values, reflecting the aggregated time–varying demand of the consumers in each area. We study the case where the components $\Delta P_{Li}(t) \neq 0$ of the disturbance vector $\Delta P_L(t)$ lie within a known interval

$$\Delta P_{Li,\min} \leq \Delta P_{Li}(t) \leq \Delta P_{Li,\max}, \quad \forall t \geq 0,$$

with $\Delta P_{Li,\min} \in \mathbb{R}_-^*,\ \Delta P_{Li,\max} \in \mathbb{R}_+^*$ being the known load bounds.

Remark 1: The assumption about "piecewise constant loads" is a realistic one, since the LFC loop is expected to act in a different time scale("much faster") than the variation of the power loads. The assumption about the loads lying in a "known interval" is also realistic since the Power Companies keep (and use for load prediction/estimation) extended logs for the time variation of the loads for each day of the year. It should also be remarked that if we are concerned with purely linear area models and controls (i.e. by neglecting amplitude and rate saturation in the control signal), it is not

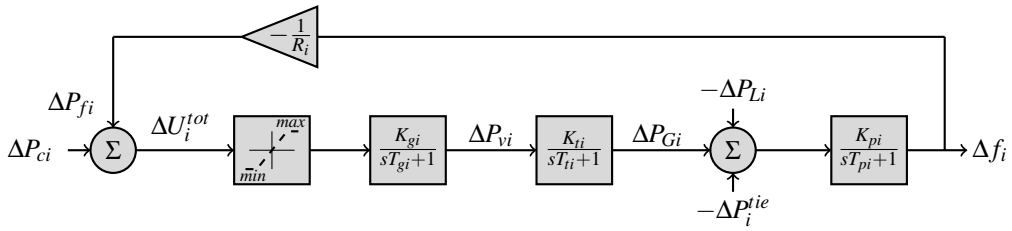

Fig. 3. Three-block model.

obligatory that the limits $\Delta P_{Li,\max}, \Delta P_{Li,\min}$ are known, since a linear controller with integral action can handle unknown step disturbances.

5) The tie–line signals ΔP_i^{tie} acting as frequency–dependent disturbances: Each control area in this N–area network can exchange power with its neighbours via (one or more) weak tie lines. The term "weak" signifies the fact that the tie-lines are usually dimensioned as a fraction of the base powers of the areas they connect. Whenever a load change occurs anywhere in the network, the power flows on the tie lines deviate from their nominal values, and the linearized dynamics of the power $\Delta P_{i,j}^{tie}$ flowing into area i from area j, using the purely reactive tie–line, is governed by

$$\begin{aligned} \Delta P_{i,j}^{tie}(t) &= 2\pi T_{ij}\int_0^t (\Delta f_i(\tau)-\Delta f_j(\tau))d\tau \\ &= K_{ij}\int_0^t (\Delta f_i(\tau)-\Delta f_j(\tau))d\tau \end{aligned} \quad (4)$$

with $K_{ij} \doteq 2\pi T_{ij}$ and T_{ij} being the synchronization coefficient between the two areas, a constant having to do with the cosine of the steady–state phase angles between the voltage phasors in the busbars connecting areas i and j [1, 2]. The synchronization coefficients satisfy $T_{ij} = T_{ji}$ (the cosine being an even function of its arguments) and if two areas are not interconnected then $T_{ij} = 0$.

The state variable associated with the tie–line interconnections of each area is the net power inflow ΔP_i^{tie} into area i (a temporary loan from all "neighbors") given by the sum

$$\Delta P_i^{tie}(t) = \sum_{j=1, j\neq i}^{n} \Delta P_{i,j}^{tie}(t) \quad (5)$$

Combining (4),(5) (and excluding the time dependence notation) the "archetypal" tie–lines power deviation dynamics, describing the power inflow into area–i via the tie–lines from all the other areas becomes

$$\Delta \dot{P}_i^{tie} = \sum_{j=1, j\neq i}^{N} K_{ij}\Delta f_i - \sum_{j=1, j\neq i}^{N} K_{ij}\Delta f_j = L_N \Delta f \quad (6)$$

or equivalently, after integrating and using a slightly abused vector notation,

$$\Delta P^{tie}(t) = L_N \int_0^t \Delta f(\tau)d\tau \quad (7)$$

with $L_N \in \mathbb{R}^{N\times N}$ being the weighted Laplacian of the network graph with edge weights K_{ij} [4, 31–34].

Remark 2: The tie–line state equations (6),(7) are independent of the model complexity used for the power area, that is they remain intact in all three models presented. Moreover, as far as the local frequency is concerned, ΔP_i^{tie} acts as a disturbance to the area and this is the reason why it contributes to ΔP^{net} with a minus sign [1–3].

6) The control signals ΔP_{ci}, ΔP_{fi}, ΔU_i^{tot} : The total control input $\Delta U_i^{tot}(t)$ is the sum of two components

$$\begin{aligned} \Delta U_i^{tot}(t) &= \Delta P_{ci}(t) + \Delta P_{fi}(t),\ i = 1, 2, \ldots, N \\ &= \Delta P_{ci}(t) - \frac{1}{R_i}\Delta f_i(t) \end{aligned} \quad (8)$$

namely the primary frequency control action $\Delta P_{fi}(t)$ and the secondary action $\Delta P_{ci}(t)$ (to be designed) which is a major function in the so called automatic generation control - "AGC"). The primary frequency control action $\Delta P_{fi}(t) = -\frac{1}{R_i}\Delta f_i(t)$, is a (preexisting) local and fast "P-type" linear control law performed by the speed governor, a regulating unit with hard constraints (mainly due to a position controlled steam valve) attached on the prime mover (steam- or hydro-turbine). The preselected static gains R_i are commonly referred to as "speed droop" or speed regulation and reflect the steady–state active power/frequency ("P–f") curves of the lumped synchronous generators [1–4].

The load fluctuations in a power network cause the electrical frequency of each area Δf_i and tie-line power inflow ΔP_i^{tie} into each area to deviate from their nominal(steady–state)values and the primary frequency control action $\Delta P_{fi}(t) = -\frac{1}{R_i}\Delta f_i(t)$, being a purely proportional local controller, cannot eliminate them. Both these deviations are instead eliminated by the secondary control action $\Delta P_c(t)$ within the so called "automatic generation control (AGC)" tier in Electric Power Systems usually implemented via a SCADA system. In the early days of LFC $\Delta P_c(t)$ was naively designed as a decentralized pure integrator or PI controller [1, 2, 19], while recently more advanced control schemes were developed and tested [3, 22].

7) The issue of control input (amplitude and rate) saturation: Although in this work speed governor dynamics are explicitly handled only in Model-3, there exists a crucial modelling and control issue arising from the inevitable hard constraint due to the steam–valve whose limited actuation can move between two limits:"fully open" and "fully closed".

In practice the total control signal $\Delta U_i^{tot}(t)$ in each area is subject to an input amplitude saturation hard constraint of the form

$$\Delta U_{i,\min}^{tot} \leq \Delta U_i^{tot}(t) \leq \Delta U_{i,\max}^{tot}, \quad \forall t \geq 0,\ i = 1, 2, \ldots, N \quad (9)$$

This saturation nonlinearity (along with generator's rate saturation (GRC) and governor's deadzone) changes qualitatively and quantitatively the whole picture in LFC as has been demonstrated in [9, 17, 18]. This important and realistic nonlinearity is not handled in this first section of this work because the focus is on linear modelling and controllability issues. In section IV though, the input saturation is taken into account and the standard H_∞ controller is enhanced with an anti–windup compensator along with a restriction on the gains' norm, as a potential remedy to its harmful effects. The important issues of generator's rate saturation (GRC) and governor's deadzone -although typical in LFC literature- are not yet covered in this work.

8) The measurement and performance signals: The vector of the measurement variables $y(t)$ is the full state vector which is assumed available for feedback control.

The performance variables $z_i(t),\ i=1,2,\ldots,n$ are a linear combination of all the signals we want to regulate in each area (i.e. the local frequency and the net power flow borrowed by the neighbor areas via the tie–lines) known in the literature as the "Area Control Error" (ACE), defined as

$$z_i(t) \doteq \beta_i \Delta f_i(t) + \Delta P_i^{tie}(t),\ \beta_i > 0,\ i=1,2,\ldots,N \qquad (10)$$

and reflecting the control objective that both these signals should asymptotically zeroed by an appropriate feedback "AGC" controller. An "optimal" choice for the frequency weighting coefficients β_i is $\beta_i = \frac{1}{K_{P_i}} + \frac{1}{R_i}$ [1, 3]. Using

$$B_z = \mathrm{diag}\Big(\beta_1,\ldots,\beta_N\Big) \qquad (11)$$

the aggregated performance vector $z = [z_1,\ z_2,\ldots,z_N]^T$ is thus

$$z = B_z \Delta f + \Delta P^{tie} \qquad (12)$$

9) Performance specifications: Following the guidelines presented in [4, 12, 19, 30], the performance specifications for the closed–loop system are set in terms of the common nominal frequency f°, the Power Base $P_{Bi}\ i=1,2,\ldots,N$ of each area, the maximum amplitude of the generated total control signal, and the settling time T_s of the system responses (frequency and tie–line power flow) as follows:

$$\begin{aligned} \Delta f_i(t) &\leq 0.2\times f^\circ \quad \forall t \\ \lim_{t\to\infty} \Delta f_i(t) &= 0 = \lim_{t\to\infty} \Delta P_i^{tie}(t) \\ T_s &\leq 20 \ \ seconds \\ \Delta P_i^{tie}(t) &\leq 0.1\times P_{Bi} \quad \forall t \\ \Delta U_{i,\min}^{tot} &\leq \Delta U_i^{tot}(t) \leq \Delta U_{i,\max}^{tot},\ \forall t \end{aligned} \qquad (13)$$

Note that the specification on $\Delta P_i^{tie}(t)$ is actually a "soft" constraint reflecting the notion of "weak" tie–lines, while the specification on $\Delta U_i^{tot}(t)$ reflects the constraints set not only by the saturators modelling the steam valves but also the thermal power limits of the lumped synchronous generators in each area.

C. The structure of the (three) state space formulations for N–areas dynamics

Using the following compact notation for the $\mathbb{R}^N$ vectors of signals

$$\begin{aligned} \Delta f &= [\Delta f_1,\ldots,\Delta f_N]^\top,\quad \int \Delta f = \int_0^t \Delta f(\tau)d\tau \\ \Delta P_G &= [\Delta P_{G1},\ldots,\Delta P_{GN}]^\top,\quad \Delta P^{tie} = \left[\Delta P_1^{tie},\ldots,\Delta P_N^{tie}\right]^\top \\ \Delta P_v &= [\Delta P_{v1},\ldots,\Delta P_{vN}]^\top,\quad \Delta U^{tot} = \left[\Delta U_1^{tot},\ldots,\Delta U_N^{tot}\right]^\top \\ \Delta P_L &= [\Delta P_{L1},\ldots,\Delta P_{LN}]^\top,\quad \Delta P_c = [\Delta P_{c1},\ldots,\Delta P_{cN}]^\top \end{aligned} \qquad (14)$$

it will be shown that, by temporarily ignoring the saturators or any other nonlinear element, the open–loop dynamics of the interconnected power system for all three models examined can be cast in the formulation:

$$\begin{aligned} S_o\ :\ \dot{x}(t) &= A_N x(t) + B_{uN}\Delta P_c(t) + B_{wN}\Delta P_L(t),\quad x(0)=x_0 \\ z(t) &= C_{zN}x(t) \\ y(t) &= x(t), \end{aligned} \qquad (15)$$

where $t\in\mathbb{R}_+$ is the time variable and the subscript N added in the system, input and disturbance matrices acts as a reminder of the number of areas we are concerned with ($N=2,3,4,\ldots$). Sections **??** and III-D offer specific examples for fully connected two area and three area systems.

The state space formulation of the three models introduced in section II-A before are derived below. The issue of controllability loss is shown and proved.

In this section it is also shown that while the graph Laplacian is the source of the controllability problem at the same time is also the solution to it.

A similarity transformation is presented which reveals the single "redundant/uncontrollable" state variable (the source of the controllability problem).

It is then shown that after reducing the dimension of the state vector, by discarding the dynamics of the single "redundant" state variable, the ensuing reduced state space representation is ALWAYS controllable and can thus be used for control design "without any loss of information".

An important remark is that **the reduced–state models, introduced further below, also conform with the above formulation** (see section III-C.2).

D. N-areas state space equations based on the three–block area model (Model-3)

The state vector $x(t) = \left[\Delta f^\top, \Delta P_G^\top, \Delta P_v^\top, (\Delta P^{tie})^\top\right]^\top \in \mathbb{R}^{4N}$ used in this modelling approach consists of the local frequency Δf_i, the local generation ΔP_{Gi}, the power generation command ΔP_{vi} to the local speed governor and the net power inflow ΔP_i^{tie} into area i.

Using the "archetypal" frequency, turbine/generator, speed–governor and tie–line state equations (3),(2),(1),(6) for

$\Delta f_i,\ \Delta P_{Gi},\ \Delta P_{vi},\ \Delta P_i^{tie}$ respectively, i.e.

$$\begin{aligned}
\Delta\dot{f}_i &= -\frac{1}{T_{pi}}\Delta f_i + \frac{K_{pi}}{T_{pi}}\left(\Delta P_{Gi} - \Delta P_i^{tie} - \Delta P_{Li}\right)\\
\Delta\dot{P}_{Gi} &= -\frac{1}{T_{ti}}\Delta P_{Gi} + \frac{K_{ti}}{T_{ti}}\Delta P_{vi}\\
\Delta\dot{P}_{vi} &= -\frac{1}{T_{gi}}\Delta P_{vi} + \frac{K_{gi}}{T_{gi}}\Delta P_{ci} - \frac{K_{gi}}{R_i T_{gi}}\Delta f_i\\
\Delta\dot{P}_i^{tie} &= \sum_{j=1,j\neq i}^{N} K_{ij}\Delta f_i - \sum_{j=1,j\neq i}^{N} K_{ij}\Delta f_j = L_N\Delta f \quad (16)
\end{aligned}$$

and introducing the ("local" to this section) matrix notation

$$\begin{aligned}
A_f &= \text{diag}\left(1/T_{p1},\ldots,1/T_{pN}\right)\\
B_f &= \text{diag}\left(K_{p1}/T_{p1},\ldots,K_{pN}/T_{pN}\right)\\
B_t &= \text{diag}\left(1/T_{t1},...,1/T_{tN}\right)\\
B_{tu} &= \text{diag}\left(K_{t1}/T_{t1},...,K_{tN}/T_{tN}\right)\\
A_g &= \text{diag}\left(K_{g1}/(R_1T_{g1}),\ldots,K_{gN}/(R_NT_{gN})\right)\\
B_g &= \text{diag}\left(1/T_{g1},...,1/T_{gN}\right)\\
B_{gu} &= \text{diag}\left(K_{g1}/T_{g1},...,K_{gN}/T_{gN}\right) \quad (17)
\end{aligned}$$

where all the above diagonal matrices $\in \mathbb{R}^{N\times N}$ are nonsingular, since all their diagonal elements are positive real numbers, a continuous-time open–loop linear state space model S_o in the form presented in (15) can be extracted. The system matrix $A_N \in \mathbb{R}^{4N\times 4N}$ and the input and disturbance matrices $B_{uN}, B_{wN}, \in \mathbb{R}^{4N\times N}$ in (15) have the following structure:

$$\begin{aligned}
A_N &= \left[\begin{array}{cccc|c} -A_f & B_f & \mathbb{O}_N & -B_f\\ \mathbb{O}_N & -B_t & B_{tu} & \mathbb{O}_{\mathbb{N}}\\ -A_g & \mathbb{O}_N & -B_g & \mathbb{O}_N\\ \hline L_N & \mathbb{O}_N & \mathbb{O}_N & \mathbb{O}_N \end{array}\right]\\
B_{uN} &= \left[\mathbb{O}_N \quad \mathbb{O}_N \quad B_{gu}^\top \quad \mathbb{O}_N\right]^\top\\
B_{wN} &= \left[-B_f \quad \mathbb{O}_N \quad \mathbb{O}_N \quad \mathbb{O}_N\right]^\top. \quad (18)
\end{aligned}$$

The performance vector can be cast as

$$z = B_z\Delta f + \Delta P^{tie} = C_{zN}\ x = [B_z \quad \mathbb{O}_N \quad \mathbb{O}_N \quad \mathbb{I}_N]\ x. \quad (19)$$

Remark 3: Note that the A_f, B_f matrices in (17) depend only the parameters of the "Area Blocks", whereas the matrices B_t, B_{tu} depend on the parameters of the turbine/generator blocks. The matrices A_g, B_g, B_{gu} on the other hand depend on the parameters of the speed governor blocks and the droop gains. It should also be noted that although the notation used in (17) is "local" to this section, the same A_f, B_f, B_t, B_{tu} matrices are also used in Model-2 below.

Proposition 1: Assume that all parameters defining the model in equation (17) are positive and that the graph is connected. Then $0 \in \lambda(A_N)$ with algebraic multiplicity one. Further 0 is an uncontrollable mode of the pair (A_N, B_{uN}) while the remaining $4N-1$ eigenvalues of A_N are controllable modes of (A_N, B_{uN}).

Proof: The proof is based on the following sequence of arguments: (i) zero is an uncontrollable mode of the pair (A_N, B_{uN}); (ii) Every nonzero eigenvalue of A_N is a controllable mode of the pair (A_N, B_{uN}); and (iii) The zero eigenvalue of A_N has algebraic multiplicity one.

(i) First note that $0 \in \lambda(A_N)$ since the last N rows of A_N are linearly dependent ($\det(L_N) = 0$). Let $1_N^\top \in \mathbb{R}^N$ be the vector with all elements equal to one. From standard properties of the Laplacian we have that $1_N^\top L_N = 0_N^\top$. Let $\xi^\top = [0_{3N}^\top \mid 1_N^\top]$. Then $\xi^\top A_N = 0_{4N}^\top$ and $\xi^\top B_{uN} = 0_N^\top$. Then the Popov-Belevitch-Hautus test implies that zero is an uncontrollable mode of (A_N, B_{uN}).

(ii) Let $\lambda_0 \in \mathbb{C}$ be an uncontrollable mode of (A_N, B_{uN}). Then there is a $\xi \in \mathbb{C}^{4N}$, $\xi \neq 0_{4N}$, such that $\xi^*[\lambda_0\mathbb{I}_{4N} - A_N \mid B_{uN}] = 0_{5N}^\top$. Write $\xi^* = [\xi_1^* \mid \xi_2^* \mid \xi_3^* \mid \xi_4^*]$, $\xi_i \in \mathbb{C}^N$ for $i = 1,2,3,4$. Then

$$\xi^* B_{uN} = 0_N^\top \Rightarrow \xi_3^* B_{gu} = 0_N^\top \Rightarrow \xi_3 = 0_N \text{ since } \det(B_{gu}) \neq 0$$

Further $\xi^*(\lambda_0\mathbb{I}_{4N} - A_N) = 0_{4N}^\top$ implies that:

$$\begin{aligned}
\xi_1^*(\lambda_0\mathbb{I}_N + A_f) - \xi_4^* L_N &= 0_N^\top\\
-\xi_1^* B_f + \xi_2^*(\lambda_0\mathbb{I}_N + B_f) &= 0_N^\top\\
-\xi_2^* B_{tu} &= 0_N^\top\\
\xi_1^* B_f + \lambda_0\xi_4^* &= 0_N^\top
\end{aligned}$$

Since $\det(B_{tu}) \neq 0$ the third equation implies that $\xi_2 = 0_N$. Then, the second equation implies that $\xi_1 = 0_N$ ($\det(B_f) \neq 0$). The first equation now gives $\xi_4^* L_N = 0$ which implies that $\xi_4^* = \mu 1_N^\top$ for some $\mu \in \mathbb{C}$, $\mu \neq 0$. (Note that the nullspace of L_N is one-dimesional and that $\xi_4 \neq 0_N$ since otherwise $\xi = 0_{4N}$). Thus, the fourth equation says that $\lambda_0\mu 1_N^\top = 0$ and hence $\lambda_0 = 0$.

(iii) Noting that $L_N = L_N^\top \geq 0$ has nullity one we can write

$$L_N = U\Lambda U^\top = \left[\begin{array}{cc} U_1 & U_2 \end{array}\right]\left[\begin{array}{cc} \Lambda_+ & 0_{N-1}\\ 0_{N-1}^\top & 0 \end{array}\right]\left[\begin{array}{c} U_1^\top\\ U_2^\top \end{array}\right]$$

where $\Lambda_+ = \text{diag}(\Lambda_+) > 0$, $U_1 \in \mathbb{R}^{N\times(N-1)}$ and $UU^\top = U^\top U = I_N$. Define the matrices:

$$P = \left[\begin{array}{cc} I_{3N} & 0_{3N,N}\\ 0_{N,3N} & U^\top \end{array}\right] \text{ and } Q = \left[\begin{array}{cccc} \mathbb{O}_N & \mathbb{O}_N & \mathbb{O}_N & U\\ \mathbb{O}_N & \mathbb{I}_N & \mathbb{O}_N & \mathbb{O}_N\\ \mathbb{O}_N & \mathbb{O}_N & I_N & \mathbb{O}_N\\ \mathbb{I}_N & \mathbb{O}_N & \mathbb{O}_N & \mathbb{O}_N \end{array}\right]$$

Consider the rank-preserving transformation $A_N \to PA_NQ$. Then

$$PA_NQ = \left[\begin{array}{cccc|c} -B_f & B_f & \mathbb{O}_N & -A_fU_1 & -A_fU_2\\ \mathbb{O}_N & -B_t & B_{tu} & 0_{N,N-1} & 0_N\\ \mathbb{O}_N & \mathbb{O}_N & -B_g & -A_gU_1 & -A_gU_2\\ 0_{N-1,N} & 0_{N-1,N} & 0_{N-1,N} & \Lambda_+ & 0_{N-1}\\ \hline 0_N^\top & 0_N^\top & 0_N^\top & 0_{N-1}^\top & 0 \end{array}\right]$$

and hence $\text{Rank}(A_N) = 4N-1$ since the matrices B_f, B_t, B_g and Λ_+ are invertible. This shows that 0 is an eigenvalue of A_N with geometric multiplicity one. To show that the algebraic multiplicity of 0 as an eigenvalue of A_N is also one, let $x = [x_1^\top\ x_2^\top\ x_3^\top\ x_4^\top]^\top \neq 0_{4N}$, $x_i \in \mathbb{R}^N$ for $i = 1,2,3,4$,

be a (right) eigenvector of A_N corresponding to the zero eigenvalue so that:

$$\begin{bmatrix} -A_f & B_f & \mathbb{O}_N & -B_f \\ \mathbb{O}_N & -B_t & B_{tu} & \mathbb{O}_N \\ -A_g & \mathbb{O}_N & -B_g & \mathbb{O}_N \\ L_N & \mathbb{O}_N & \mathbb{O}_N & \mathbb{O}_N \end{bmatrix} \begin{bmatrix} x_1 \\ x_2 \\ x_3 \\ x_4 \end{bmatrix} = 0_{4N}$$

which implies that

$$\begin{aligned} -A_f x_1 + B_f x_2 - B_f x_4 &= 0_N \\ -B_t x_2 + B_{tu} x_3 &= 0_N \\ -A_g x_1 - B_g x_3 &= 0_N \\ L_N x_1 &= 0_N \end{aligned}$$

Note that $x_1 \neq 0_N$, for otherwise the third equation implies that $x_3 = 0_N$ (since $\det(B_g) \neq 0$); the second equation then implies that $x_2 = 0_N$ ($\det(B_t) \neq 0$), while the first equation in turn implies that $x_4 = 0_N$ (since $\det(B_f) \neq 0$). Thus $x_1 = 0_N$ implies that $x = 0_{4N}$, which is a contradiction.

Thus $x_1 \neq 0_N$ and hence without loss of generality we can write $x_1 = 1_N$ from the fourth equation above. This implies in turn that:

$$x_3 = -B_g^{-1} A_g 1_N, \;\; x_2 = -B_t^{-1} B_{tu} B_g^{-1} A_g 1_N$$

and

$$x_4 = -(B_f^{-1} A_f + B_t^{-1} B_{tu} B_g^{-1} A_g) 1_N$$

and hence

$$x = \begin{bmatrix} \mathbb{I}_N \\ -B_t^{-1} B_{tu} B_g^{-1} A_g \\ -B_g^{-1} A_g \\ -(B_f^{-1} A_f + B_t^{-1} B_{tu} B_g^{-1} A_g) \end{bmatrix} 1_N$$

spans the (one-dimensional) eigenspace of A_N corresponding to the zero eigenvalue (i.e. the null-space of A_N). Suppose now that the algebraic multiplicity of the zero eigenvalue is larger than one. Then there would exist a generalized eigenvector $y = [y_1^\top \; y_2^\top \; y_3^\top \; y_4^\top]^\top$, $y_i \in \mathbb{R}^N$ for $i = 1,2,3,4$, such that

$$A_N \begin{bmatrix} x & y \end{bmatrix} = \begin{bmatrix} x & y \end{bmatrix} \begin{bmatrix} 0 & 1 \\ 0 & 0 \end{bmatrix}$$

or equivalently

$$A_N x = 0 \;\text{ and }\; A_N y = x$$

Pre-multiply the two terms in the second equation by:

$$\beta^\top = \begin{bmatrix} 0_N^\top & 0_N^\top & 0_N^\top & 1_N^\top \end{bmatrix}$$

The left-hand-side term, $\beta^\top A_N y$, is equal to zero. The right-hand-side term

$$\begin{aligned} \beta^\top x &= -1_N^\top \left(B_f^{-1} A_f + B_t^{-1} B_{tu} B_g^{-1} A_g \right) 1_N \\ &= -\sum_{k=1}^{N} (B_f^{-1} A_f + B_t^{-1} B_{tu} B_g^{-1} A_g)_{kk} < 0 \end{aligned}$$

which establishes a contradiction and concludes the proof. ■

Remark 4: The matrix A_N is singular because the Laplacian matrix L_N located in the $(3,1)$ block position of A_N (next to a block of zeros) is rank-deficient and hence its spectrum always contains zero as an eigenvalue; this has algebraic multiplicity one since it is assumed that the graph describing the network is connected [31, 32]. Note that the corresponding zero eigenvalue of A_N is uncontrollable both from the control and the load disturbance input (see third block rows of zeros in both the input matrices B_{uN} and B_{wN}). Thus, although this mode lies on the boundary of the stability region it cannot cause internal stability problems to the system. However, it may cause technical problems with the application of optimal control methods (e.g. LQR or $\mathscr{H}_\infty$) which rely on a Riccati equation whose stabilising solution is guaranteed to exist under the assumption that the pair (A_N, B_{uN}) is free of uncontrollable modes on the imaginary axis.

In the following proposition a controllable state-space model is derived by transforming the original model in Kalman canonical form. It is shown that the minimal model can be described by a subset of the original state variables.

Proposition 2: Consider the model defined in equations (15) and (18)–(19). An equivalent reduced-order model is given by:

$$\dot{\psi} = \hat{A}_N \psi + \hat{B}_{uN} \Delta P_C + \hat{B}_{wN} \Delta P_L, \;\; z = B_z \Delta f + \begin{bmatrix} \mathbb{I}_{N-1} \\ -1_{N-1}^\top \end{bmatrix} \Delta \hat{P}^{tie}$$

in which

$$\psi = \begin{bmatrix} \Delta f \\ \Delta P_G \\ \Delta P_v \\ \Delta \hat{P}^{tie} \end{bmatrix}, \;\; \Delta \hat{P}^{tie} = \begin{bmatrix} \Delta P_1^{tie} & \Delta P_2^{tie} & \cdots & \Delta P_{N-1}^{tie} \end{bmatrix}^\top$$

Also,

$$\hat{A}_N = \begin{bmatrix} -A_f & B_f & \mathbb{O}_N & -B_f \begin{bmatrix} \mathbb{I}_{N-1} \\ -1_{N-1}^\top \end{bmatrix} \\ \mathbb{O}_N & -B_t & B_{tu} & 0_{N,N-1} \\ -A_g & \mathbb{O}_N & -B_g & 0_{N,N-1} \\ \begin{bmatrix} \mathbb{I}_{N-1} & 0_{N-1} \end{bmatrix} L_N & 0_{N-1,N} & 0_{N-1,N} & \mathbb{O}_{N-1} \end{bmatrix}$$

and

$$\hat{B}_{uN} = \begin{bmatrix} \mathbb{O}_N \\ \mathbb{O}_N \\ B_{tu} \\ 0_{N-1,N} \end{bmatrix}, \;\; \hat{B}_{wN} = \begin{bmatrix} -B_f \\ \mathbb{O}_N \\ \mathbb{O}_N \\ 0_{N-1,N} \end{bmatrix}$$

Further the pair $(\hat{A}_N, \hat{B}_{uN})$ is controllable.

Proof: Consider the state-space model defined in (15) and (18)–(19) and let x be the corresponding state-vector:

$$x = \begin{bmatrix} (\Delta f)^\top & (\Delta P_G)^\top & (\Delta P_v)^\top & (\Delta P^{tie})^\top \end{bmatrix}^\top$$

Define the state-space transformation $\xi = T_N x$ where $T_N \in \mathbb{R}^{3N \times 3N}$ is

$$T_N = \begin{bmatrix} \mathbb{I}_{3N} & 0_{3N,N} \\ 0_{N,3N} & \Psi_N \end{bmatrix}, \Psi_N = \begin{bmatrix} \mathbb{I}_{N-1} & 0_{N-1} \\ 1_{N-1}^\top & 1 \end{bmatrix} \tag{20}$$

and note that the inverse of T_N is:

$$T_N^{-1} = \begin{bmatrix} \mathbb{I}_{3N} & 0_{3N,N} \\ 0_{N,3N} & \Psi_N^{-1} \end{bmatrix}, \Psi_N^{-1} = \begin{bmatrix} \mathbb{I}_{N-1} & 0_{N-1} \\ -1_{N-1}^\top & 1 \end{bmatrix} \quad (21)$$

The open–loop N-Area dynamics in (15) is then transformed to:

$$\dot{\xi}(t) = \tilde{A}_N \xi(t) + \tilde{B}_{uN} \Delta P_c(t) + \tilde{B}_{wN} \Delta P_L(t) \quad (22)$$

with

$$\tilde{B}_{uN} = T_N B_{uN} = B_{uN}, \ \tilde{B}_{wN} = T_N B_{wN} = B_{wN} \quad (23)$$

and setting $\tilde{A}_N := T_N A_N T_N^{-1}$,

$$\tilde{A}_N = \left[\begin{array}{ccc|c} -A_f & B_f & \mathbb{O}_N & -B_f \Psi_N^{-1} \\ \mathbb{O}_N & -B_t & B_{tu} & \mathbb{O}_N \\ -A_g & \mathbb{O}_N & -B_g & \mathbb{O}_N \\ \hline \Psi_N L_N & \mathbb{O}_N & \mathbb{O}_N & \mathbb{O}_N \end{array}\right] \quad (24)$$

Note that the first $4N-1$ variables of state vectors $x(t)$ and $\xi(t)$ in the original and transformed coordinates are identical, whereas the last element of ξ, ξ_{4N}, is:

$$\xi_{4N}(t) = \sum_{i=1}^{N} \Delta P_i^{tie}(t) = 0 \text{ for all } t \geq 0$$

Further, since the last row of $\Psi_N L_N$ is equal to $1_N^\top L_N = 0_N^\top$, the last row of $\tilde{A}_N$ is zero. Since this is also true for the last rows of B_{uN} and B_{wN}, the last ODE in (22) can be written as:

$$\dot{\xi}_{4N} = 0 \Rightarrow \xi_{4N}(t) = \xi_{4N}(0) = 0 \text{ for all } t \geq 0$$

for all control and disturbance signals $\Delta P_c(t)$ and $\Delta P_L(t)$, $t \geq 0$. Thus the last equation in (22) is trivial (identity) and can be eliminated from the model by removing the last rows of $\tilde{A}_N$, $\tilde{B}_{uN}$ and $\tilde{B}_{wN}$. Similarly, since $\xi_{4N}(t) = 0$ for all $t \geq 0$, the last column of $\tilde{A}_N$ can also be eliminated, resulting in the minimal realization given in the statement of the Proposition. Finally the performance vector can be written as a linear combination of the new state variables:

$$z = B_z \Delta f + \Delta P^{tie} = B_z \Delta f + \begin{bmatrix} \mathbb{I}_{N-1} \\ -1_{N-1}^\top \end{bmatrix} \Delta \hat{P}^{tie}$$

as required. ∎

Remark 5: Matrix T_N acting on the state vector $x = \left[(\Delta f)^\top \ (\Delta P_G)^\top \ (\Delta P_v)^\top \ (\Delta P^{tie})^\top\right]^\top$ to produce ξ, leaves the first three vectors intact. Further, its action on the fourth vector $\Delta P^{tie} = \left[\Delta P_1^{tie}, \ldots, \Delta P_N^{tie}\right]^\top$ leaves the first $N-1$ variables $\{\Delta P_i^{tie} : i = 1, 2, \ldots, N-1\}$ intact and replaces the last state variable, ΔP_N^{tie}, by $\sum_{i=1}^N \Delta P_i^{tie}$. Thus the model retains its physical significance as the state variables in the initial and transformed coordinates are essentially the same. Further, the last transformed variable, $\sum_{i=1}^N \Delta P_i^{tie}$, is identically zero. This follows from the reciprocal relationships:

$$\Delta P_{i,j}^{tie} = -\Delta P_{j,i}^{tie}$$

which imply that

$$\sum_{i=1}^{N} \Delta P_i^{tie} = \sum_{i=1}^{N} \sum_{j=1, j \neq i} \Delta P_{i,j}^{tie} = 0$$

for fully connected networks and more generally for networks with undirected graphs:

$$\sum_{i=1}^{N} \Delta P_i^{tie} = \sum_{i=1}^{N} \sum_{j \in \mathcal{N}_i} \Delta P_{i,j}^{tie} = 0$$

where $\mathcal{N}_i$ denotes the set of neighbours of area i. Formally, the fact that the last transformed variable is zero can be seen from the last row of the product $\Psi_N L_N$ (in the $(4,1)$ block position of the transformed matrix $\tilde{A}_N$) which is zero since 1_N spans the null-space of L_N. Since the last row of the transformed input matrices $\tilde{B}_{uN}$ and $\tilde{B}_{wN}$ remains zero, the last state equation in the transformed coordinates is trivial and can be removed, resulting in the minimal state-space model with $4N-1$ variables given in the proposition statement. Note that there is nothing special about agent N in this approach - in principle any other ΔP_i^{tie} variable could have been eliminated (or, equivalently, the agents could have been re-labelled).

E. N-areas state space equations based on the two–block area model (Model-2)

For Model-2 the stable governor dynamics are assumed infinitely fast with $K_{gi} = 1$ and $T_{gi} = 0$ (transfer function$= 1$), hence $\Delta P_{vi} = \Delta U_i^{tot}$ and the "archetypal" turbine/generator dynamics (2) (without any type of nonlinearity considered yet) becomes

$$\begin{aligned} \Delta \dot{P}_{Gi} &= -\frac{1}{T_{ti}} \Delta P_{Gi} + \frac{K_{ti}}{T_{ti}} \Delta U_i^{tot} \\ &= \left(-\frac{K_{ti}}{R_i T_{ti}}\right) \Delta f_i - \frac{1}{T_{ti}} \Delta P_{Gi} + \frac{K_{ti}}{T_{ti}} \Delta P_{ci} \end{aligned} \quad (25)$$

The state vector $x(t) = \left[\Delta f^\top, \Delta P_G^\top, (\Delta P^{tie})^\top\right]^\top \in \mathbb{R}^{3N}$ used in this modelling approach consists of the local frequency Δf_i, the local generation ΔP_{Gi}, and the net power inflow ΔP_i^{tie} into area i and a continuous-time open–loop linear state space model S_o in the form presented in (15) can be extracted for the N-areas linearized system. Indeed using the "archetypal" frequency, turbine/generator and tie–line state equations (3),(25), (6) for Δf_i, ΔP_{Gi}, ΔP_i^{tie} respectively, the system matrix $A_N \in \mathbb{R}^{3N \times 3N}$ in (15) has the following structure

$$A_N = \left[\begin{array}{cc|c} -A_f & B_f & -B_f \\ -A_t & -B_t & \mathbb{O}_N \\ \hline L_N & \mathbb{O}_N & \mathbb{O}_N \end{array}\right] \quad (26)$$

with

$$A_t = \text{diag}\left(K_{t1}/(R_1 T_{t1}), \ldots, K_{tN}/(R_N T_{tN})\right) \quad (27)$$

and the same definitions for the A_f, B_f, B_t, B_{tu} matrices given in (17). The input and disturbance matrices $B_{uN}, B_{wN}, \in \mathbb{R}^{3N \times N}$ write as

$$\begin{aligned} B_{uN} &= \begin{bmatrix} \mathbb{O}_N & B_{tu}^\top & \mathbb{O}_N \end{bmatrix}^\top, \\ B_{wN} &= \begin{bmatrix} -B_f^\top & \mathbb{O}_N & \mathbb{O}_N \end{bmatrix}^\top \end{aligned} \quad (28)$$

and the performance vector as

$$z = B_z \Delta f + \Delta P^{tie} = C_{zN} \ x = [B_z \quad \mathbb{O}_N \quad \mathbb{I}_N] \ x. \quad (29)$$

Proposition 3: Assume that all parameters defining the model (A_N, B_{uN}) in equations (26) and (28) are positive and that the graph is connected. Then $0 \in \lambda(A_N)$ with algebraic multiplicity one. Further 0 is an uncontrollable mode of the pair (A_N, B_{uN}) while the remaining $3N-1$ eigenvalues of A_N are controllable modes of (A_N, B_{uN}).

Proof: The proof is almost identical to the proof of Proposition 1 and therefore omitted. ∎

In the following proposition a controllable state-space model is derived by transforming the original model in Kalman canonical form. The minimal model is again described by a subset of the original state variables.

Proposition 4: Consider the model defined in equations (15) and (26)–(29). An equivalent reduced-order model is given by:

$$\dot{\psi} = \hat{A}_N \psi + \hat{B}_{uN} \Delta P_C + \hat{B}_{wN} \Delta P_L, \; z = B_z \Delta f + \begin{bmatrix} \mathbb{I}_{N-1} \\ -1_{N-1}^\top \end{bmatrix} \Delta \hat{P}^{tie}$$

in which

$$\psi = \begin{bmatrix} \Delta f \\ \Delta P_G \\ \Delta \hat{P}^{tie} \end{bmatrix}, \quad \Delta \hat{P}^{tie} = \begin{bmatrix} \Delta P_1^{tie} & \Delta P_2^{tie} & \cdots & \Delta P_{N-1}^{tie} \end{bmatrix}^\top$$

Also,

$$\hat{A}_N = \begin{bmatrix} & -A_f & B_f & -B_f \begin{bmatrix} \mathbb{I}_{N-1} \\ -1_{N-1}^\top \end{bmatrix} \\ & -A_t & -B_t & 0_{N,N-1} \\ \begin{bmatrix} \mathbb{I}_{N-1} & 0_{N-1} \end{bmatrix} L_N & 0_{N-1,N} & & \mathbb{O}_{N-1} \end{bmatrix}$$

and

$$\hat{B}_{uN} = \begin{bmatrix} \mathbb{O}_N \\ B_{tu} \\ 0_{N-1,N} \end{bmatrix}, \; \hat{B}_{wN} = \begin{bmatrix} -B_f \\ \mathbb{O}_N \\ 0_{N-1,N} \end{bmatrix}$$

Further the pair $(\hat{A}_N, \hat{B}_{uN})$ is controllable.

Proof: The proof is again similar to the proof of Proposition (2) and therefore omitted. ∎

F. N-areas state space equations based on the single–block area model (Model-1)

Starting with Model-2, the Model-1 is derived by assuming that the stable turbine/generator dynamics are infinitely fast with $K_{ti} = 1$ and $T_{ti} = 0$ (transfer function= 1), hence ΔP_{Gi} coincides with the total control signal i.e. $\Delta P_{Gi}(t) = \Delta U_i^{tot}(t) = \Delta P_{ci}(t) - \frac{1}{R_i}\Delta f_i(t)$ from (8) the "archetypal" frequency state equations (3) become

$$\begin{aligned} \dot{\Delta f_i} &= -\frac{1}{T_{pi}}\Delta f_i + \frac{K_{pi}}{T_{pi}}(\Delta P_{ci} - \frac{1}{R_i}\Delta f_i) - \frac{K_{pi}}{T_{pi}}\Delta P_i^{tie} - \frac{K_{pi}}{T_{pi}}\Delta P_{Li} \\ &= -\Big(\frac{1}{T_{pi}}(1 + \frac{K_{pi}}{R_i})\Big)\Delta f_i + \frac{K_{pi}}{T_{pi}}\Delta P_{ci} - \frac{K_{pi}}{T_{pi}}\Delta P_i^{tie} - \frac{K_{pi}}{T_{pi}}\Delta P_{Li} \end{aligned}$$

The state vector $x(t) = \left[\Delta f^\top \quad (\Delta P^{tie})^\top\right]^\top \in \mathbb{R}^{2N}$ used in this modelling approach consists of the local frequency Δf_i,and the net power inflow ΔP_i^{tie} into area i. Combining with the tie–line dynamics in (6) the "Model-1 LFC dynamics" is cast in the state–space formulation presented in (15). Indeed, introducing the diagonal matrices (the notation being "local" to this section)

$$\begin{aligned} A_f &= \text{diag}\Big(\frac{1}{T_{p1}}(1 + \frac{K_{p1}}{R_1}), \ldots, \frac{1}{T_{pN}}(1 + \frac{K_{pN}}{R_N})\Big) \\ B_f &= \text{diag}\Big(K_{p1}/T_{p1}, \ldots, K_{pN}/T_{pN}\Big) \end{aligned} \tag{30}$$

with the the system matrix $A_N \in \mathbb{R}^{2N \times 2N}$ being

$$A_N = \left[\begin{array}{c|c} -A_f & -B_f \\ \hline L_N & \mathbb{O}_N \end{array}\right], \tag{31}$$

the input and disturbance matrices $B_{uN}, B_{wN}, \in \mathbb{R}^{2N \times N}$ being

$$B_{uN} = \begin{bmatrix} B_f \\ \mathbb{O}_N \end{bmatrix}, \; B_{wN} = \begin{bmatrix} -B_f \\ \mathbb{O}_N \end{bmatrix} \tag{32}$$

and the performance vector expressed as

$$z = B_z \Delta f + \Delta P^{tie} = C_{zN}\, x = [B_z \quad \mathbb{I}_N]\; x. \tag{33}$$

Note that both A_f, B_f matrices in (30), and consequently also the system and input matrices A_N, B_{uN}, B_{wN}, depend only the parameters of the "Area Blocks" and the droop gains.

Remark 6: The important remark here is that the matrix pair $\{A_N, B_{uN}\}$ in (31),(32) **is not controllable** due to the Laplacian being positive semidefinite (its spectrum always contains a zero eigenvalue) [31, 32] ...and the zero submatrices next to it ...and the corresponding zero submatrices in B_{uN}... ...hence there is always an uncontrollable eigenvalue at the origin.... and the realization is **non-minimal.**

Proof: It is easy to see that the corresponding nonsingular similarity transformation matrix $T_N \in \mathbb{R}^{2N \times 2N}$ for the Model-1 approach is

$$T_N = \begin{bmatrix} \mathbb{I}_N & \mathbb{O}_N \\ \mathbb{O}_N & \Psi_N \end{bmatrix}, \Psi_N = \begin{bmatrix} \mathbb{I}_{N-1} & 0_{N-1} \\ 1_{N-1}^\top & 1 \end{bmatrix}$$

and its inverse is

$$T_N^{-1} = \begin{bmatrix} \mathbb{I}_N & \mathbb{O}_N \\ \mathbb{O}_N & \Psi_N^{-1} \end{bmatrix}, \Psi_N^{-1} = \begin{bmatrix} \mathbb{I}_{N-1} & 0_{N-1} \\ -1_{N-1}^\top & 1 \end{bmatrix} \tag{34}$$

■

Remark 7: Similar structured representations of the linearized LFC dynamics (possibly with different state variable ordering or different selection of state variables) have been recently used in the context of Distributed/Decentralized LFC design and the detection of data corruption attacks on cyber–physical power systems [4, 12, 33–37]. If for example the state vector x is chosen as in [36]

$$x = \left[\int \Delta f^\top \;\; \Delta f^\top\right]^\top \tag{35}$$

it can be easily checked that, due to (6), the state space formulation conforms with the one in (15) using the same A_f, B_f matrices as in (30) with the matrices $A_N, B_{uN}, B_{wN}, C_{zN}$ now being

$$\begin{aligned} A_N &= \begin{bmatrix} \mathbb{O}_N & \mathbb{I}_N \\ -B_f L_N & -A_f \end{bmatrix}, \; B_{uN} = \begin{bmatrix} \mathbb{O}_N \\ B_f \end{bmatrix}, \\ B_{wN} &= \begin{bmatrix} \mathbb{O}_N \\ -B_f \end{bmatrix}, \; C_{zN} = \begin{bmatrix} L_N & B_z \end{bmatrix} \end{aligned} \tag{36}$$

A nonsingular similarity transformation relates the state space representations in (36) and (31),(32).

Very often in the LFC literature the "swing equation" is used as a modelling starting point especially for the design of distributed LFC laws, with the vector of rotor angles $\delta(t)$ in each area being part of the state vector [4, 33–35]. This formulation can be shown to be equivalent with our "Model-1" approach once we recall that the time derivative of the rotor angle is the rotor speed deviation in electrical radians per second i.e.

$$\dot{\delta}(t) = \Delta\omega(t) = \omega(t) - \omega_{ref} = 2\pi\big(\Delta f(t) - \Delta f_{ref}\big) = 2\pi\Delta f(t)$$

Hence the following state vector used in [4, 33–35]

$$\big[\delta^\top \ \Delta\omega^\top\big]^\top = \big[\int \Delta\omega^\top \ \Delta\omega^\top\big]^\top \tag{37}$$

is of course equivalent to the one presented in (35).

III. Exploiting the Modelling, Controllability and Model Reduction Results for Load Frequency Control Design (Ignoring Input Saturation)

A. Integral control action enforced via state augmentation

It is well known that the easiest way to enforce integral action is to "artificially" augment the system dynamics with extra state variables being equal to the time integral of the signals to be regulated. Such an approach guarantees asymptotic regulation (set–point tracking) in the presence of piecewise constant disturbances (reference signals) [38, 39]. In our case, for all three models, the extra state variables needed for state augmentation are encapsulated in the vector $x_I \in \mathbb{R}^{N_z}$ defined as the integral of the performance signal "Area Control Error" (ACE) i.e.

$$\dot{x}_I(t) = z(t) = C_z x(t) = ACE(t) \Rightarrow x_I(t) = \int_0^t z(\tau)d\tau \tag{38}$$

The augmented dynamics S_a can then be expressed as

$$\begin{aligned} S_a \ : \ \dot{x}_a(t) &= A_a x_a(t) + B_{u,a}\Delta P_c(t) + B_{w,a}\Delta P_L(t), \\ z(t) &= C_{z,a} x_a(t) \end{aligned} \tag{39}$$

where the subscript "a" signifies the augmented version of each vector or matrix in (15) e.g.

$$A_a \doteq \begin{bmatrix} A_N & 0_{N_x,N_z} \\ C_{zN} & 0_{N_z} \end{bmatrix}, \quad B_{u,a} = \begin{bmatrix} B_{uN} \\ 0_{N_z,N_u} \end{bmatrix} \tag{40}$$

where the zero matrices appearing are of appropriate dimensions.

It is now clear that designing of a static state–feedback regulator $\Delta P_c(t) = K_a x_a(t)$ for the augmented system (39) will provide an AGC controller consisting of two parts: the desired integral action, assuring a zero steady state (ACE) error despite the presence of the unknown piecewise constant disturbances, and a regulating state feedback term which focuses on the performance criteria. Figure 4 depicts the proposed control architecture for the designed AGC control.

$$\Delta P_c(t) = K_a x_a(t) = K_x x(t) + K_I \int_0^t z(\tau)d\tau \tag{41}$$

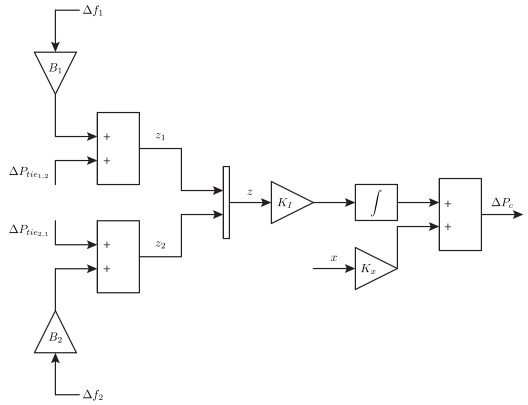

Fig. 4. The proposed Control architecture (state feedback and integral action) for two areas.

Next we investigate the controllability properties of the system augmented with integrator dynamics. Augmentation introduces N eigenvalues at the origin. Thus, if the non-minimal model is used for augmentation purposes the augmented system has $N+1$ zero modes, one of which is uncontrollable (i.e. the uncontrollable mode at the origin is inherited by the augmented system). The presence of this uncontrollable mode at the origin is highly undesirable since it cannot be moved by state-feedback and hence the system is strictly speaking not stabilisable. This phenomenon can manifest itself during the design phase (numerically even, in the presence of a mode of this type which is "almost uncontrollable"). For example, it is well known that a necessary condition in LQR design for the existence of a stabilizing solution to the corresponding Algebraic Riccati Equation (ARE) which defines the optimal state-feedback is that the pair of state matrices (A,B) is free of uncontrollable modes on the imaginary axis. It is shown in the sequel that in the present case if the minimal model is used the N modes at the origin introduced by augmentation are always controllable. This is true irrespective of the complexity of the model at node-level (i.e. irrespective of whether the one-state, two-state or three-state node model is used) as long as all parameters are non-trivial (positive) and the graph of the interconnected network is connected, i.e. $\text{Rank}(L_N) = N-1$. This result is derived next for the three-state node-model case and is based on the following Proposition:

Proposition 5: Consider the augmented system

$$\begin{bmatrix} \dot{x} \\ \dot{z} \end{bmatrix} = \begin{bmatrix} A & 0_{n,p} \\ -C & \mathbb{O}_p \end{bmatrix} \begin{bmatrix} x \\ z \end{bmatrix} + \begin{bmatrix} B \\ 0_{p,m} \end{bmatrix} u$$

where $A \in \mathbb{R}^{n\times n}$, $B \in \mathbb{R}^{n\times m}$, $C \in \mathbb{R}^{p\times n}$ and $p \le m$. Then the system is controllable if and only if: (i) (A,B) is controllable, and (ii)

$$\text{Rank}\left(\begin{bmatrix} A & B \\ -C & 0_{p,m} \end{bmatrix}\right) = n + p$$

Proof: See Willems [**?**]. A slightly simpler proof based on Popov-Belevitch-Hautus test is included here.

Sufficiency: Suppose that the pair

$$\left(\left[\begin{array}{cc} A & 0_{n,p} \\ -C & \mathbb{O}_p \end{array} \right], \left[\begin{array}{c} B \\ 0_{p,m} \end{array} \right] \right)$$

is controllable. Then

$$\text{Rank} \left(\left[\begin{array}{cc|c} s\mathbb{I}_n - A & 0_{n,p} & B \\ C & s\mathbb{I}_p & 0_{p,m} \end{array} \right] \right) = n+m+p$$

for all $s \in \mathbb{C}$. Equivalently:

$$\left[\begin{array}{cc} \xi_1^\top & \xi_2^\top \end{array} \right] \left[\begin{array}{cc|c} s\mathbb{I}_n - A & 0_{n,p} & B \\ C & s\mathbb{I}_p & 0_{p,m} \end{array} \right] \neq 0_{n+m+p}^\top$$

for all $s \in \mathbb{C}$, $[\xi_1^\top \ \xi_2^\top]^\top \neq 0_{n+p}$. This implies that

$$\left[\begin{array}{cc} \xi_1^\top & 0_p^\top \end{array} \right] \left[\begin{array}{cc|c} s\mathbb{I}_n - A & 0_{n,p} & B \\ C & s\mathbb{I}_p & 0_{p,m} \end{array} \right] \neq 0_{n+m+p}^\top$$

for all $s \in \mathbb{C}$ and $\xi_1 \neq 0_n$, i.e.

$$\xi_1^\top \left[\begin{array}{c|c} s\mathbb{I}_n - A & B \end{array} \right] \neq 0_{n+m}^\top$$

for all $s \in \mathbb{C}$ and $\xi_1 \neq 0_n$ which implies (i). In addition, setting $s = 0$ gives:

$$\left[\begin{array}{cc} \xi_1^\top & \xi_2^\top \end{array} \right] \left[\begin{array}{cc|c} -A & 0_{n,p} & B \\ C & \mathbb{O}_p & 0_{p,m} \end{array} \right] \neq 0_{n+m+p}^\top$$

for all $[\xi_1^\top \ \xi_2^\top]^\top \neq 0_{n+p}$. Equivalently:

$$\left[\begin{array}{cc} \xi_1^\top & \xi_2^\top \end{array} \right] \left[\begin{array}{cc} A & B \\ -C & 0_{p,m} \end{array} \right] \neq 0_{n+m}^\top$$

for all $[\xi_1^\top \ \xi_2^\top]^\top \neq 0_{n+p}$, which implies (ii).

Necessity: Suppose that (i) and (ii) hold but the pair

$$\left(\left[\begin{array}{cc} A & 0_{n,p} \\ -C & \mathbb{O}_p \end{array} \right], \left[\begin{array}{c} B \\ 0_{p,m} \end{array} \right] \right)$$

is uncontrollable. Then there exists $[\xi_1^\top \ \xi_2^\top]^\top \neq 0_{n+p}$, $\lambda \in \sigma(A)$ such that:

$$\left[\begin{array}{cc} \xi_1^\top & \xi_2^\top \end{array} \right] \left[\begin{array}{cc|c} \lambda\mathbb{I}_n - A & 0_{n,p} & B \\ C & \lambda\mathbb{I}_p & 0_{p,m} \end{array} \right] = 0_{n+m+p}^\top$$

Hence

$$\begin{aligned} \xi_1^\top(\lambda\mathbb{I}_n - A) + \xi_2^\top C &= 0_n^\top \\ \lambda\xi_2^\top &= 0_p^\top \\ \xi_1^\top B &= 0_m^\top \end{aligned}$$

If $\lambda \neq 0$ then $\xi_2 = 0_p$ which implies that

$$\xi_1^\top(\lambda\mathbb{I}_n - A) = 0_n^\top \ \text{ and } \ \xi_1^\top B = 0_m^\top$$

contradicting (i). If $\lambda = 0$ then

$$\left[\begin{array}{cc} \xi_1^\top & \xi_2^\top \end{array} \right] \left[\begin{array}{cc} A & B \\ -C & 0_{p,m} \end{array} \right] = 0_{n+m}^\top$$

contradicting (ii). This concludes the proof. ∎

Proposition 6: Consider the system $(\hat{A}_N, \hat{B}_{uN})$ defined in Proposition 2. Assume that all model parameters are positive and the graph of the network is connected (so that $\text{Rank}(L_N) = N-1$). Define also the corresponding (output) matrix:

$$\hat{C}_{zN} = \left[\begin{array}{cccc} B_z & \mathbb{O}_N & \mathbb{O}_N & \left[\begin{array}{c} \mathbb{I}_{N-1} \\ -1_{N-1}^T \end{array} \right] \end{array} \right]$$

(which maps the state of the model to the performance variable) where B_z is defined in equation (11). Then the augmented system $(\hat{A}_a, \hat{B}_a)$, where

$$\hat{A}_a = \left[\begin{array}{cc} \hat{A}_N & 0_{4N-1,N} \\ \hat{C}_{zN} & \mathbb{O}_N \end{array} \right], \ \text{and} \ \hat{B}_a = \left[\begin{array}{c} \hat{B}_{uN} \\ \mathbb{O}_N \end{array} \right]$$

is controllable.

Proof: First note that since the number of rows of $\hat{C}_{zN}$ is equal to the number of columns of $\hat{B}_{uN}$ Proposition 5 is applicable. In particular, to prove the result it suffices to show that:

$$\text{Rank}(\Phi) = 5N-1, \ \ \Phi := \left[\begin{array}{cc} \hat{A}_N & \hat{B}_{uN} \\ \hat{C}_{zN} & \mathbb{O}_N \end{array} \right]$$

Equivalently is suffices to prove the implication $\xi^\top\Phi = 0_{5N-1}^\top \Rightarrow \xi = 0_{5N-1}$. Let

$$\xi^\top = \left[\begin{array}{ccccc} \xi_1^\top & \xi_2^\top & \xi_3^\top & \xi_4^\top & \xi_5^\top \end{array} \right]$$

where $\xi_i \in \mathbb{R}^N$, $i = 1,2,3,5$ and $\xi_4 \in \mathbb{R}^{N-1}$. Then $\xi^\top\Phi = 0_{5N-1}^\top$ is equivalent to the set of equations:

$$\begin{aligned} &\xi_1^\top A_f + \xi_3^\top A_g - \xi_4^\top \left[\begin{array}{c|c} \mathbb{I}_{N-1} & 0_{N-1} \end{array} \right] L_N - \xi_5^\top B_z = 0_N^\top \\ &\xi_1^\top B_f - \xi_2^\top B_t = 0_N^\top \\ &\xi_2^\top B_{tu} - \xi_3^\top B_g = 0_N^\top \\ &\xi_1^\top B_f \left[\begin{array}{c} \mathbb{I}_{N-1} \\ -1_{N-1}^\top \end{array} \right] - \xi_5^\top \left[\begin{array}{c} \mathbb{I}_{N-1} \\ -1_{N-1}^\top \end{array} \right] = 0_{N-1}^\top \\ &\xi_3^\top B_{tu} = 0_N^\top \end{aligned}$$

Since B_{tu} is nonsingular the last equation implies that $\xi_3 = 0_N$. Then the third equation implies that $\xi_2 = 0_N$ (B_{tu} nonsingular) from which the second equation gives $\xi_1 = 0_N$ (B_f nonsingular). Thus equation $\xi^\top\Phi = 0_{5N-1}^\top$ is equivalent to $\xi_1 = \xi_2 = \xi_3 = 0_N$ together with the following two equations:

$$\xi_4^\top \left[\begin{array}{c|c} \mathbb{I}_{N-1} & 0_{N-1} \end{array} \right] L_N + \xi_5^\top B_z = 0_N^\top \tag{42}$$

and

$$\xi_5^\top \left[\begin{array}{c} \mathbb{I}_{N-1} \\ -1_{N-1}^\top \end{array} \right] = 0_{N-1}^\top \tag{43}$$

Write $\xi_5^\top = [\xi_{51}^\top \mid \xi_{52}]$ where $\xi_{51} \in \mathbb{R}^{N-1}$ and $\xi_{52} \in \mathbb{R}$. Then equation (43) implies that $\xi_{51}^\top = \xi_{52} 1_{N-1}^\top$ and hence

$$\xi_5^\top = \left[\begin{array}{cc} \xi_{52} 1_{N-1}^\top & \xi_{52} \end{array} \right] = \xi_{52} 1_N^\top \tag{44}$$

Write

$$L_N = \left[\begin{array}{c} \hat{L}_{N-1} \\ l_N^\top \end{array} \right], \ \hat{L}_{N-1} \in \mathbb{R}^{(N-1)\times N}, \ l_N \in \mathbb{R}^N \tag{45}$$

Then equations (42), (45) and (44) imply that:

$$\xi_4^\top \hat{L}_{N-1} + \xi_{52} 1_N^\top B_z = 0$$

Multiplying from the left by 1_N while noting that $\hat{L}_{N-1}1_N = 0_{N-1}$ gives:

$$\xi_{52}1_N^\top B_z 1_N = \xi_{52}\sum_{i=1}^{N}\beta_i = \xi_{52}\sum_{i=1}^{N}\left(\frac{1}{k_{P_i}}+\frac{1}{R_i}\right) = 0$$

which implies that $\xi_{52} = 0$ and hence from equation (44) that $\xi_5^\top = \xi_{52}1_N^\top = 0_N^\top$. It remains to show that $\xi_4 = 0_{N-1}$. Define the eigenvalue decomposition of L_N:

$$L_N = \begin{bmatrix} U_1 & u_N \end{bmatrix}\begin{bmatrix} \Lambda_+ & 0_{N-1} \\ 0_{N-1}^\top & 0 \end{bmatrix}\begin{bmatrix} U_1^\top \\ u_N^\top \end{bmatrix} = \sum_{i=1}^{N-1}\lambda_i u_i u_i^\top$$

in which

$$U_1 = \begin{bmatrix} u_1 & \cdots & u_{N-1} \end{bmatrix} \in \mathbb{R}^{N\times(N-1)},\ U = \begin{bmatrix} U_1 & u_N \end{bmatrix}$$

and

$$UU^\top = U^\top U = \mathbb{I}_N,\ \Lambda_+ = \mathrm{diag}(\lambda_1,\lambda_2,\ldots,\lambda_{N-1})$$

with $\lambda_i > 0,\ i = 1,2,\ldots,N-1$. Write $u_i^\top = [u_{i1}^\top \mid u_{i2}]^\top$, $i = 1,2,\ldots,N$, where $u_{i1} \in \mathbb{R}^{N-1}$ and $u_{i2} \in \mathbb{R}$. Then from equation (42) and the fact that $\xi_5 = 0_N$:

$$\begin{bmatrix} \xi_4^\top & 0 \end{bmatrix} L_N = 0 \Rightarrow \sum_{i=1}^{N-1}\lambda_i(\xi_4^\top u_{i1})u_i^\top = 0$$

Multiplying from the right by $u_j,\ j \in \{1,2,\ldots,N-1\}$ and using the orthonormality property of the eigenvectors we get:

$$\lambda_j(\xi_4^\top u_{j1}) = 0 \Rightarrow \xi_4^\top u_{j1} = 0$$

since $\lambda_j > 0$. Repeating the argument for all $j = 1,2,\ldots,N-1$ gives

$$[\xi_4^\top \mid 0]\begin{bmatrix} u_1 & u_2 & \ldots & u_{N-1} \end{bmatrix} = [\xi_4^\top \mid 0]U_1 = 0_{N-1}^\top$$

Thus vector $[\xi_4^\top \mid 0]^\top$ is orthogonal to the subspace spanned by the orthonormal vectors $\{u_i\}_{i=1}^{N-1}$ and thus $[\xi_4^\top|0]^\top = \mu u_n$ for some $\mu \in \mathbb{R}$, i.e. $[\xi_4^\top \mid 0]^\top$ lies in the (one dimensional) null-space of L_n. Since the null space of L_N, however, is spanned by the vector 1_N we must have $\mu = 0$ and hence $\xi_4 = 0_{N-1}$. Thus $\xi = 0_{5N-1}$ which concludes the proof. ■

B. Linear (LMI based) LFC design combining H_∞ and Pole Clustering

The design methodology for H_∞ and pole clustering Static State Feedback (SSF) control synthesis for the LFC problem, has been described quite extensively in [3, 9, 11, 29] and only a brief description of the proposed approach will be given here.

It is well known that for a generic Linear Time Invariant system $\{A, B_u, B_w, C_z\}$, like the one in (15), the search for a stabilizing static state–feedback (SSF) $u(t) = Kx(t)$ guaranteeing an optimum H_∞ norm γ, corresponding to an optimum level of disturbance attenuation $\|z\|_2/\|\Delta P_L\|_2 < \gamma$, is equivalent (if and only if) with the existence of a symmetric positive definite matrix X and a matrix Y such that the following matrix inequality holds [40]

$$\begin{bmatrix} \Lambda+\Lambda^T & B_w & XC_z^T \\ B_w^T & -\gamma I_{N_w} & 0_{N_z,N_w} \\ C_zX & 0_{N_w,N_z} & -\gamma I_{N_z} \end{bmatrix} < 0$$
$$X > 0 \qquad (46)$$

where N_w, N_z are the dimensions of the disturbance vector ΔP_L and the performance variable vector z respectively, and $\Lambda(X,Y) \doteq AX + B_uY$. If LMI (46) has a feasible solution (in terms of X, Y, γ), the SSF control gain $K = YX^{-1}$ stabilizes the closed loop system while minimizing the disturbance effect on the performance channel in the sense of "γ-attenuation" explained before.

On the other hand, the set of the three synthesis LMIs D_α, D_r, D_θ for a state feedback controller $u = Kx$ placing the closed poles inside a prespecified convex LMI region $D(\alpha, r, \theta)$, are given below with the decision variables being the symmetric positive definite matrix X and the matrix Y.

$$\begin{aligned} D_\alpha(X,Y) &: 2\alpha X + \Lambda + \Lambda^T < 0,\ \text{with } X = X^T > 0 \\ D_r(X,Y) &: \begin{bmatrix} -rX & \Lambda^T \\ \Lambda & -rX \end{bmatrix} < 0 \\ D_\theta(X,Y) &: \begin{bmatrix} \sin\theta[\Lambda+\Lambda^T] & \cos\theta[-(\Lambda)+\Lambda^T] \\ (*)^T & \sin\theta[\Lambda+\Lambda^T] \end{bmatrix} < 0 \end{aligned} \qquad (47)$$

where again $\Lambda(X,Y) = AX + B_uY$ and the controller gain is computed as $K = YX^{-1}$ [9, 11, 16, 41]. Now the two sets of LMIs (46) and (47), reflecting respectively disturbance attenuation and transient performance control objectives, can be combined into one LMI by demanding that the decision variables X, Y appearing in each set are common.

C. A fully interconnected TWO AREA example

A fully interconnected two–area example is used in this section as a "step–by–step" example of the generic ("N-areas") state space formulation and and control methodologies provided. The Model-2 formulation, being "right in the middle" of the model complexity scale, was chosen (without loss of generality) to exemplify the modelling concepts and control design methodologies presented so far. The results can be easily extrapolated to the other two modelling approaches.

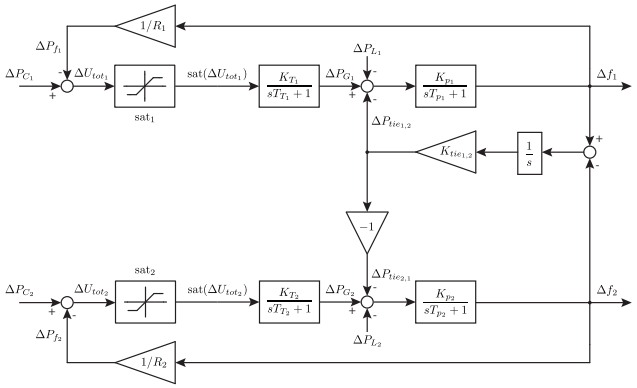

Fig. 5. Block-diagram of a two–area power system (with input saturation)

.

The block diagram of the linearized (open–loop) for a two–area Model-2 power network is shown in Figure 5. A detailed explanation of all individual parameters involved in

the block diagram along with their corresponding values and units is provided in Table I in the simulation section III-C.

Starting with the tie–line dynamics it should be recalled that the state–space presented below is common for all three models (Models-$1,2,3$) presented, hence it is also valid for the chosen Model-2.

$$\begin{aligned}\Delta\dot{P}_1^{tie} &= K_{12}\Delta f_1 - K_{12}\Delta f_2 \\ \Delta\dot{P}_2^{tie} &= -K_{21}\Delta f_1 + K_{21}\Delta f_2 \end{aligned} \tag{48}$$

Since $K_{12}=K_{21}$ it is clear that $\Delta P_2^{tie} = K_{21}(\Delta f_2 - \Delta f_1) = -\Delta P_1^{tie}$ which has two consequencies: (i) ΔP_2^{tie} for the specific two–area benchmark system is redundant (i.e. it does not offer any information to be used for feedback control) (ii) ΔP_2^{tie} cannot be controlled "independently" of ΔP_1^{tie}, a clear sign of controllability loss.

The performance variables $z_i(t),\ i=1,2$ are defined as $z_1(t)=\beta_1\Delta f_1(t)+\Delta P_1^{tie}$ and $z_2(t)=\beta_2\Delta f_2(t)+\Delta P_2^{tie} = \beta_2\Delta f_2(t)-\Delta P_1^{tie}$.

1) Using the FULL (6–state–variable) state vector Controllability is Lost : The formulation of the state equations in the generic form presented in (15) for the "full" (6–state–variable) state vector $x(t)\in\mathbb{R}^6$

$$x = \begin{bmatrix}\Delta f_1 & \Delta f_2 & \Delta P_{G1} & \Delta P_{G2} & \Delta P_1^{tie} & \Delta P_2^{tie}\end{bmatrix}^\top$$

is straightforward, with the structure of the ensuing A_2 system matrix being

$$A_2 = \left[\begin{array}{cc|cc|cc} -\frac{1}{T_{p1}} & 0 & \frac{K_{p1}}{T_{p1}} & 0 & -\frac{K_{p1}}{T_{p1}} & 0 \\ 0 & -\frac{1}{T_{p2}} & 0 & \frac{K_{p2}}{T_{p2}} & 0 & -\frac{K_{p2}}{T_{p2}} \\ \hline -\frac{K_{t1}}{R_1T_{t1}} & 0 & -\frac{1}{T_{t1}} & 0 & 0 & 0 \\ 0 & -\frac{K_{t2}}{R_2T_{t2}} & 0 & -\frac{1}{T_{t2}} & 0 & 0 \\ \hline K_{12} & -K_{12} & 0 & 0 & 0 & 0 \\ -K_{21} & K_{21} & 0 & 0 & 0 & 0 \end{array}\right] \tag{49}$$

Note the inclusion of the redundant state variable ΔP_2^{tie}. The input, disturbance and performance matrices are

$$\begin{aligned} B_{u2} &= \begin{bmatrix} 0 & 0 & \frac{K_{t1}}{T_{t1}} & 0 & 0 & 0 \\ 0 & 0 & 0 & \frac{K_{t2}}{T_{t2}} & 0 & 0 \end{bmatrix}^\top, \\ B_{w2} &= \begin{bmatrix} -\frac{K_{p1}}{T_{p1}} & 0 & 0 & 0 & 0 & 0 \\ 0 & -\frac{K_{p2}}{T_{p2}} & 0 & 0 & 0 & 0 \end{bmatrix}^\top, \\ C_{z2} &= \begin{bmatrix} \beta_1 & 0 & 0 & 0 & 1 & 0 \\ 0 & \beta_2 & 0 & 0 & 0 & 1 \end{bmatrix}^\top, \end{aligned} \tag{50}$$

As can easily be checked, both numerically and symbolically, the matrix pair $\{A_2, B_{u2}\}$ in (49),(50) is not controllable and for reasons already explained includes one uncontrollable pole at the origin, whereas the state space realization is non–minimal. The loss of controllability can be intuitively understood after realizing that the two tie–line power flows are linearly dependent signals since $\Delta P_2^{tie}(t)+\Delta P_1^{tie}(t)=0,\ \forall t$ and hence they cannot be independently controlled by the control signals $\Delta P_{c1}, \Delta P_{c2}$.

2) Revealing the redundancy and producing the REDUCED (5–state–variable) state vector: Controllability is Regained: The similarity transformation that reveals the uncontrollable mode in the two–areas Model-2 example is $\xi = T_2 x$ with matrix T_2 being

$$T_2 = \begin{bmatrix} \mathbb{I}_4 & 0_{4,2} \\ 0_{2,4} & \left[\begin{array}{c|c} 1 & 0 \\ \hline 1 & 1 \end{array}\right] \end{bmatrix}, T_2^{-1} = \begin{bmatrix} \mathbb{I}_4 & 0_{4,2} \\ 0_{2,4} & \left[\begin{array}{c|c} 1 & 0 \\ \hline -1 & 1 \end{array}\right] \end{bmatrix},$$

and the transformed system matrix $\tilde{A}_2 = T_2 A_N T_2^{-1}$ is

$$\tilde{A}_2 = \left[\begin{array}{cc|cc|cc} -\frac{1}{T_{p1}} & 0 & \frac{K_{p1}}{T_{p1}} & 0 & -\frac{K_{p1}}{T_{p1}} & 0 \\ 0 & -\frac{1}{T_{p2}} & 0 & \frac{K_{p2}}{T_{p2}} & \frac{K_{p2}}{T_{p2}} & -\frac{K_{p2}}{T_{p2}} \\ \hline -\frac{K_{t1}}{R_1T_{t1}} & 0 & -\frac{1}{T_{t1}} & 0 & 0 & 0 \\ 0 & -\frac{K_{t2}}{R_2T_{t2}} & 0 & -\frac{1}{T_{t2}} & 0 & 0 \\ \hline K_{12} & -K_{12} & 0 & 0 & 0 & 0 \\ 0 & 0 & 0 & 0 & 0 & 0 \end{array}\right]$$

while

$$\tilde{C}_{z2} = \begin{bmatrix} B_z & \mathbb{O}_2 & \Psi_2^{-1} \end{bmatrix}$$

Since the last rows of $B_{u2}=\tilde{B}_{u2}$ and $B_{w2}=\tilde{B}_{w2}$ in (50) are rows of zeros, it is clear that the last (sixth) state variable, assuming zero initial condition, is identically zero. Moreover the dynamics of $\Delta\tilde{f}_2 = \Delta f_2$ are not influenced from the presence of the non–zero element $-\frac{K_{p2}}{T_{p2}}$ in the last place of the second row of $\tilde{A}_2$ (element $2,6$), since the corresponding state variable is zero for all time $t\geq 0$. Thus, as was intuitively expected from the discussion about the "redundant" state variable ΔP_2^{tie}, there will be no loss of information after excluding the last (sixth) rows and columns of $\tilde{A}_2$, the last rows of B_{u2}, B_{w2} and the last column of $\tilde{C}_{z2}$, i.e. by introducing the reduced state vector $x_{red}(t)\in\mathbb{R}^5$,

$$x_{red} = \begin{bmatrix}\Delta f_1 & \Delta f_2 & \Delta P_{G1} & \Delta P_{G2} & \Delta P_1^{tie}\end{bmatrix}^\top \tag{51}$$

and the corresponding "reduced order" matrices

$$\begin{aligned} A_{2,red} &= \begin{bmatrix} -\frac{1}{T_{p1}} & 0 & \frac{K_{p1}}{T_{p1}} & 0 & -\frac{K_{p1}}{T_{p1}} \\ 0 & -\frac{1}{T_{p2}} & 0 & \frac{K_{p2}}{T_{p2}} & \frac{K_{p2}}{T_{p2}} \\ -\frac{K_{t1}}{R_1T_{t1}} & 0 & -\frac{1}{T_{t1}} & 0 & 0 \\ 0 & -\frac{K_{t2}}{R_2T_{t2}} & 0 & -\frac{1}{T_{t2}} & 0 \\ K_{12} & -K_{12} & 0 & 0 & 0 \end{bmatrix} \\ B_{u2,red} &= \begin{bmatrix} 0 & 0 & \frac{K_{t1}}{T_{t1}} & 0 & 0 \\ 0 & 0 & 0 & \frac{K_{t2}}{T_{t2}} & 0 \end{bmatrix}^\top, \\ B_{w2,red} &= \begin{bmatrix} -\frac{K_{p1}}{T_{p1}} & 0 & 0 & 0 & 0 \\ 0 & -\frac{K_{p2}}{T_{p2}} & 0 & 0 & 0 \end{bmatrix}^\top, \\ C_{z2,red} &= \begin{bmatrix} \beta_1 & 0 & 0 & 0 & 1 \\ 0 & \beta_2 & 0 & 0 & -1 \end{bmatrix}^\top \end{aligned} \tag{52}$$

This is a state–space representation equivalent (no loss of information) with the original full–state representation, also complying with the formulation (15), which moreover is

controllable and can be used for aggressive controller design as done in [7–11].

It should be recalled that, as already proven, the performance vector z is the same for both the full–state and the reduced–state representations. Matrix $C_{z2,red}$ in (52) fully reconstructs the performance vector z using x_{red} and hence there is no need to discriminate between z_{red} and z.

Note that for the simulation experiments the two interconnected areas were taken to be completely identical, with equal parameters for each subsystem and thus $K_{p1} = K_{p2} = K_p$, $K_{t1} = K_{t2} = K_t$, $T_{p1} = T_{p2} = T_p$ and so on. This symmetry comes without any loss of generality and makes the interpretation of the responses easily understandable. Table I provides the parameter values used for simulations [1, 6–8]

TABLE I

PARAMETER VALUES FOR EACH CONTROL AREA OF FIGURE 5 [1, 8].)

Parameter	Symbol	Value	Units
Nominal Frequency	f°	50	Hz
Power Base	P_B	2000	MW
Load Dependency Factor	D	16.66	MW/Hz
Speed Droop	R	1.2×10^{-3}	Hz/MW
Generator Inertia Constant	H	5	s
Governor Static Gain	K_g	1	MW/MW
Governor Time Constant	T_g	0.08	s
Turbine Static Gain	K_t	1	MW/MW
Turbine Time Constant	T_t	0.3	s
Area Static Gain	K_p	0.06	Hz/MW
Area Time Constant	T_p	24	s
Tie–Line Coefficient	K_{tie}	1090	MW/Hz

The "optimal" choice for the coefficients β_i has been shown to be $\beta_i = D_i + \frac{1}{R_i} = \frac{1}{K_{pi}} + \frac{1}{R_i}$ [1, 3, 8]) while for completeness, we also provide the formulas associated with the area gains K_{pi} and time constants T_{pi} as

$$K_{pi} = \frac{1}{D_i}, \quad T_{pi} = \frac{2HP_B}{f^\circ D_i}. \tag{53}$$

In all following simulations, the load bounds $\Delta P_{Li,\min} \in \mathbb{R}^*_-$ and $\Delta P_{Li,\max} \in \mathbb{R}^*_+$ were assumed to be step functions assigned to their maximum expected values of $\Delta P_{L1} = \Delta P_{L2} = +200\ MW$. The step times are different for each load in order to present the realistic event where the loads hit the network at different time instances. Thus the step time of ΔP_{L1} was set at $t = 0$ whereas for ΔP_{L2} the step change occurs at $t = 5$s.

For state augmentation two extra state variables have to be added, the time integrals of the areas' control errors $z_i(t) = ACE_i(t) = B_i\Delta f_i(t) + \Delta P_i^{tie}(t)$, and the augmented state vector $x_a(t)$ is

$$\left[\Delta f_1 \quad \Delta f_2 \quad \Delta P_{G1} \quad \Delta P_{G2} \quad \Delta P_1^{tie} \Delta P_2^{tie} \quad \int_0^t z_1(\tau)d\tau \quad \int_0^t z_2(\tau)d\tau\right]^\top$$

No constraints in the amplitude or the rate of any signal in the loop were considered, while the control methodology followed was the set of H_∞ and the pole clustering control synthesis LMIs in (46) and (47).

3) LFC using H_∞/Pole Clustering Objectives and Model-2 Full State Vector : Using the full (6–state–variable) state vector $x(t) \in \mathbb{R}^6$, and the parameters in Table I, the 6 open–loop eigenvalues of A_2 given in (49) are

$$-1.8693, \quad -1.6875 \pm 2.0581i, \quad -0.7528 \pm 3.0253i, \quad 0$$

indicating that the system is "marginally stable" due to the pole at the origin. The controllability test for the matrix pair $\{A_2, B_{u2}\}$ verifies (numerically) that, as expected, the system in not controllable, with the loss of controllability stemming from the "inevitable uncontrollable pole at the origin" due to the Laplacian. The same controllability result holds for the augmented system (39), where as also expected the matrix pair $\{A_{a2}, B_{u,a2}\}$ in (40) is not controllable. Yet it is possible to design state feedback controllers based on H_∞ methodologies provided that the control objective respects the uncontrollable pole at the origin.

Indeed the pure H_∞ (without pole clustering) control synthesis LMI in (46), for the augmented (8–state–variable) system is a feasible LMI optimization problem, achieving high disturbance attenuation as indicated from the value of $\gamma_{opt} = 0.2266$. The 8 closed–loop eigenvalues are given below without any simulation results due to space limitations.

$$-10.1149 \pm 23.6329i, \quad -8.4925 \pm 25.2030i, \quad -2.2053, \quad -0.0025, \quad -0.0025, \quad 0$$

Next, the combined H_∞ and pole clustering synthesis LMIs (46) and (47) were applied on the augmented system being feasible only for $\alpha = 0$ and infeasible for all other $\alpha > 0$.

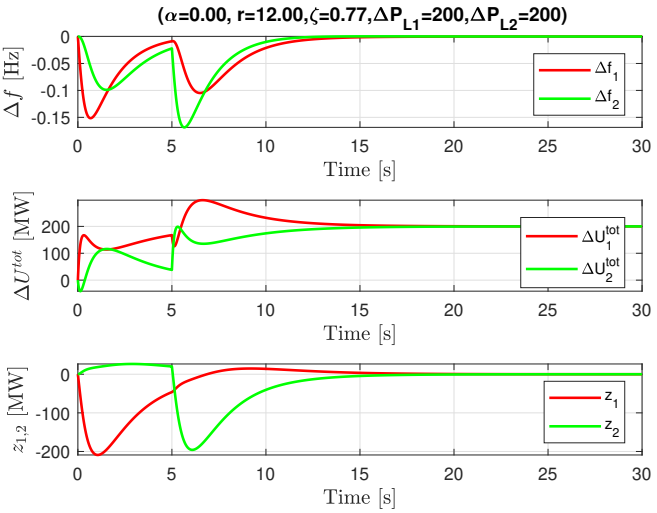

Fig. 6. $\Delta f_{1,2}(t)$, $\Delta U^{tot}_{1,2}(t)$, $z_{1,2}(t)$ responses with H_∞ control, Pole Clustering within the LMI region ($\alpha = 0, r = 12, \theta = 40^\circ$) and large loads $\Delta P_{L1} = \Delta P_{L2} = 200\ MW$ 2–Areas/2–Block/Full–State/$\alpha = 0$.

Figure 6 depicts the system responses of Area1 (red) and Area2 (green) with H_∞ control and pole clustering inside the convex LMI region with $\alpha = 0$ and $r = 12$, $\theta = 40^\circ$. The choice $\theta = 40^\circ$ corresponds to a minimum requirement of 0.77 for the damping ratios ζ, while the choice $r = 12$ corresponds to a maximum allowable requirement of 7.7rad/s

for the damped frequency. The value $\gamma_{opt} = 8.5855$ yielded by the combined LMI feasibility problem indicates a smaller disturbance attenuation capability (the price to be paid for pole clustering), while the 8 closed–loop eigenvalues are now

$$-7.8113,\ -6.8149,\ -3.1078,\ -1.6962$$
$$-1.5406,\ -0.6399,\ -0.3804,\ 0.$$

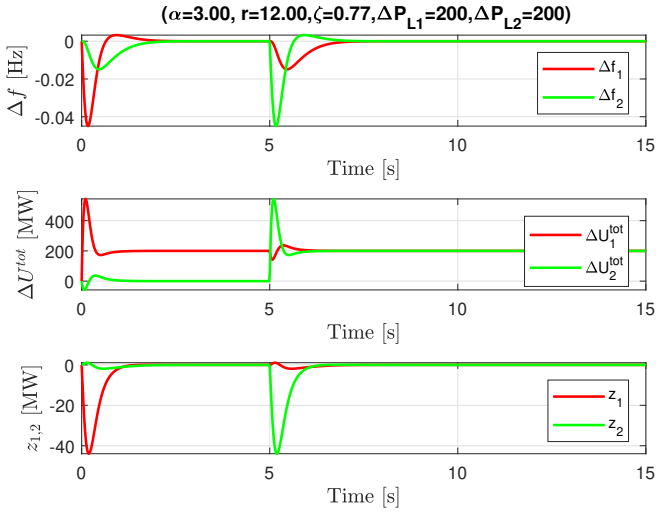

Fig. 7. $\Delta f_{1,2}(t)$, $\Delta U^{tot}_{1,2}(t)$, $z_{1,2}(t)$ responses with H_∞ control, Pole Clustering within the LMI region ($\alpha = 3, r = 12, \theta = 40^\circ$) and large loads $\Delta P_{L1} = \Delta P_{L2} = 200$ *MW* 2–Areas/2–Block/Reduced–State/$\alpha = 3$.

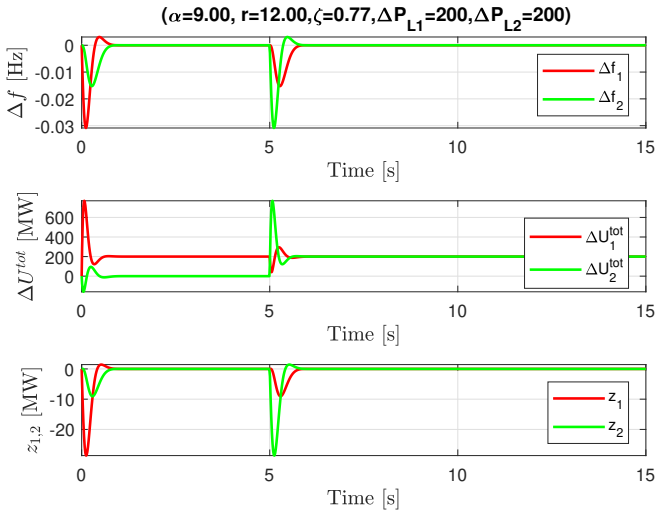

Fig. 8. $\Delta f_{1,2}(t)$, $\Delta U^{tot}_{1,2}(t)$, $z_{1,2}(t)$ responses with H_∞ control, Pole Clustering within the LMI region ($\alpha = 9, r = 12, \theta = 40^\circ$) and large loads $\Delta P_{L1} = \Delta P_{L2} = 200$ *MW* 2–Areas/2–Block/Reduced–State/$\alpha = 9$.

4) LFC using H_∞/Pole Clustering Objectives and Model-2 Reduced State Vector : Before proceeding with the presentation of the simulation results it is important to clarify that (i) the control design procedure for this case is based on the reduced–state state–space models (with the performance vector z being the same as that of the full-state model) and generates "reduced feedback gains" (lower dimension for the state feedback gain), (ii) the ensuing control signal is implemented using the reduced state vector and is applied to the full–state model.

Exploiting the fact that Pole Clustering is now feasible for all $\alpha \geq 0$, and choosing an LMI region with minimum decay rate $\alpha = 3$ and $r = 12,\ \theta = 40^\circ$, the set of LMIs is feasible, and Figure 7 depicts the achieved closed–loop system responses ($\Delta f_{1,2}(t)$) and the total control signals $\Delta U^{tot}_{1,2}(t)$. The achieved attenuation was $\gamma^{reduced}_{opt} = 0.4776$, while the 7 closed–loop eigenvalues are now

$$-9.4483 \pm 7.0296i,\ -9.5827 \pm 6.0040i,\ -3.6811$$
$$-3.1900 \pm 1.0194i.$$

with their real parts being less than -3 as prescribed.

Figure 8 depicts the closed–loop system responses for an aggressive choice with minimum decay rate $\alpha = 9$ and $r = 12,\ \theta = 40^\circ$. The settling time is very small but the control signals are extremely large, especially right after the loads hit any of the three areas.

D. A fully interconnected THREE AREA example

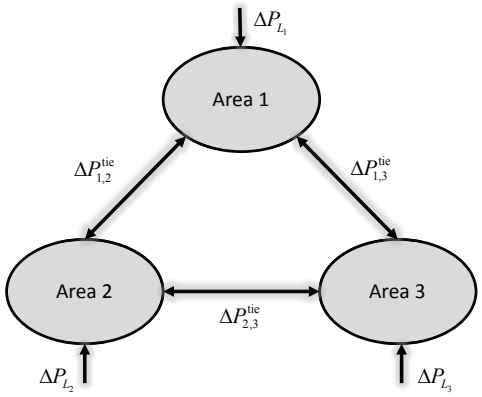

Fig. 9. Block-diagram of a fully connected three–area power system

.

The block diagram of a fully interconnected three–area power network is shown in Figure 9. Its Model-2 state space representation both in its full–state and reduced–state version will be used both for modelling and control design. The provided formulation can be easily extrapolated to the other two modelling approaches.

The state equations for frequency and turbine/generator deviations for the full–state Model-2 state space representation are readily derived from (3),(25) respectively and will not be repeated. Only the tie–line dynamics will be presented with the sole purpose to depict the structure of the weighted graph Laplacian for this non–trivial fully interconnected three areas power network. Indeed using (6) the tie–line state equations, being the same for all three models (Models-1,2,3), write as

$$\begin{aligned}
\Delta\dot{P}^{tie}_1 &= (K_{12}+K_{13})\Delta f_1 - K_{12}\Delta f_2 - K_{13}\Delta f_3 \\
\Delta\dot{P}^{tie}_2 &= (K_{21}+K_{23})\Delta f_2 - K_{21}\Delta f_1 - K_{23}\Delta f_3 \\
\Delta\dot{P}^{tie}_3 &= (K_{31}+K_{32})\Delta f_3 - K_{31}\Delta f_1 - K_{32}\Delta f_2 \qquad (54)
\end{aligned}$$

or (in compact notation using $\Delta P^{tie} = \left[\Delta P_1^{tie},\ \Delta P_2^{tie},\ \Delta P_3^{tie}\right]^\top$ and $\Delta f = [\Delta f_1,\ \Delta f_2,\ f_3]^\top$)

$$\Delta \dot{P}_i^{tie} = L_3 \Delta f$$

with the weighted Laplacian $L_3 \in \mathbb{R}^3$ (with edge weights K_{ij}) clearly being

$$L_3 = \begin{bmatrix} K_{12}+K_{13} & -K_{12} & -K_{13} \\ -K_{21} & K_{21}+K_{23} & -K_{23} \\ -K_{31} & -K_{32} & K_{31}+K_{32}. \end{bmatrix}$$

For the simulation experiments the three fully interconnected areas were assumed completely identical, with the same (equal) parameters for each subsystem using Table I, and thus $K_{p1} = K_{p2} = K_{p3} = K_p$, $K_{t1} = K_{t2} = K_{t3} = K_t$, $T_{p1} = T_{p2} = T_{p3} = T_p$ and so on. This symmetry comes without any loss of generality. No constraints in the amplitude or the rate of any signal in the loop were considered, while the control methodology followed was the set of H_∞ and the pole clustering control synthesis LMIs in (46) and (47). The step times for the three loads $\Delta P_{L1} = \Delta P_{L2} = \Delta P_{L3} = 200$ MW were set at $t = 1, 5, 9$ s respectively.

1) Using the uncontrollable FULL state vector (9–state–variable/Model-2) for LFC using H_∞/Pole Clustering Objectives: The controllability test for the matrix pair $\{A_3, B_{u3}\}$ verifies (numerically) that, as expected, the system in not controllable. The loss of controllability stems from the "inevitable uncontrollable pole at the origin" due to the graph Laplacian as explained before. So, just like the two areas full state example, the control synthesis LMIs are feasible only if the pole clustering objective respects the presence of the uncontrollable eigenvalue at the origin i.e. feasibility is guaranteed only for LMI regions with $\alpha = 0$.

Figure 10 shows the frequency deviations $\Delta f_{1,2,3}(t)$, the total control action $\Delta U^{tot}_{1,2,3}(t)$ and the performance variables ("ACEs") $z_{1,2,3}(t)$ of Area1,Area2 and Area3 with H_∞ control and pole clustering inside the convex LMI region with $\alpha = 0$ and $r = 12,\ \theta = 40^\circ$ The achieved attenuation was $\gamma_{opt} = 4.3636$. The settling time is within prescribed limits and the steady state errors are zero.

2) Revealing and Using the controllable REDUCED state vector (8–state–variable/Model-2) for LFC using H_∞/Pole Clustering Objectives: The similarity transformation is $\xi = T_3 x$ with the nonsingular matrix T_3 being

$$T_3 = \left[\begin{array}{c|c} \mathbb{I}_6 & 0_{6,3} \\ \hline 0_{3,6} & \left[\begin{array}{ccc} 1 & 0 & 0 \\ 0 & 1 & 0 \\ \hline 1 & 1 & 1 \end{array}\right] \end{array}\right], T_3^{-1} = \left[\begin{array}{c|c} \mathbb{I}_6 & 0_{6,3} \\ \hline 0_{3,6} & \left[\begin{array}{ccc} 1 & 0 & 0 \\ 0 & 0 & 0 \\ \hline -1 & -1 & 1 \end{array}\right] \end{array}\right]$$

For the LMI region with $\alpha = 3$ and $r = 12,\ \theta = 40^\circ$, using the reduced sate model for control design, the system responses are shown in Figure 11, while Figure 12 shows the responses for an aggressive choice of LMI region with $\alpha = 9$. In both cases the settling time is within prescribed limits and the steady state errors are zero, but for $\alpha = 9$ the control signals are extremely large, especially after the loads hit any of the three areas.

TAKE A LOOK AT THE APPENDIX FOR MORE SIMULATION RESULTS...

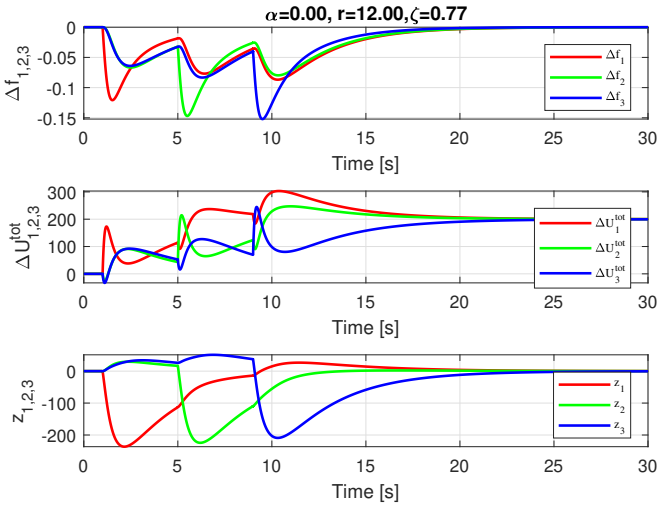

Fig. 10. $\Delta f_{1,2,3}(t)$, $\Delta U^{tot}_{1,2,3}(t)$ and $z_{1,2,3}(t)$ responses with H_∞ control and Pole Clustering within the LMI region ($\alpha = 0,\ r = 12,\ \theta = 40^\circ$ and large loads $\Delta P_{L1} = \Delta P_{L2} = \Delta P_{L3} = 200$ MW 3–Areas/2–Block/Full–State/$\alpha = 0$

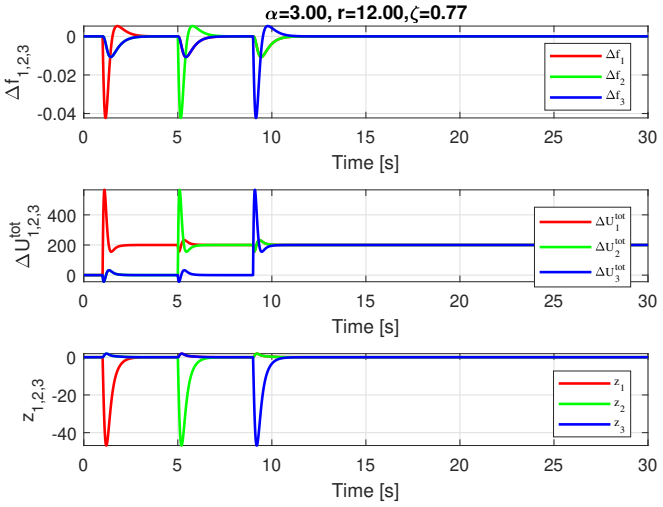

Fig. 11. $\Delta f_{1,2,3}(t)$, $\Delta U^{tot}_{1,2,3}(t)$ and $z_{1,2,3}(t)$ responses with H_∞ control and Pole Clustering within the LMI region ($\alpha = 3,\ r = 12,\ \theta = 40^\circ$) and large loads $\Delta P_{L1} = \Delta P_{L2} = \Delta P_{L3} = 200$ MW 3–Areas/2–Block/Reduce–State/$\alpha = 3$.

IV. The Performance Deterioration Arising from Input (Amplitude) Saturation in the Total Control Signal $\Delta U_i^{tot}(t)$ - How to Handle via Gain Norm Minimization and Anti–Windup Compensation

A. The perplexities arising by neglecting the (inevitable) input saturators in a purely linear controller design

The starting point in this section is that, as already mentioned in the presentation of the speed governor dynamics, in reality the total control signal $\Delta U_i^{tot}(t)$ in each area is subject to a hard amplitude input saturation constraint of the form

$$\Delta U^{tot}_{i,\min} \le \Delta U_i^{tot}(t) \le \Delta U^{tot}_{i,\max}, \quad \forall t \ge 0,\ i = 1, 2, \ldots, N \quad (55)$$

On the other hand, a control engineer with "purely linear mentality", is tempted to "make the LFC response faster" by

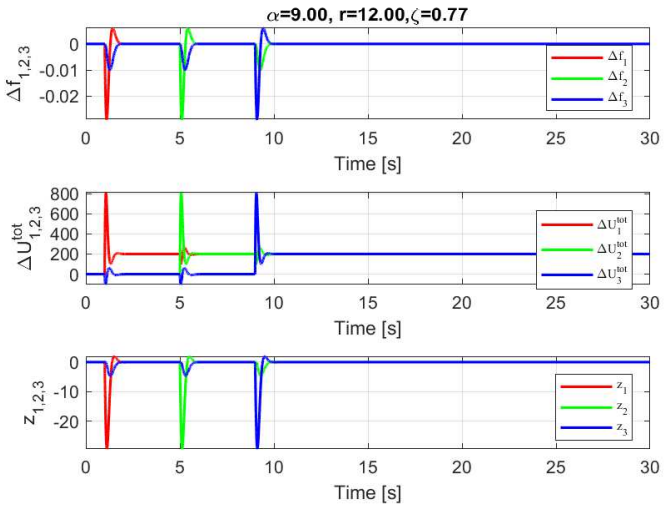

Fig. 12. $\Delta f_{1,2,3}(t)$, $z_{1,2,3}(t)$ responses with H_∞ control and Pole Clustering within the LMI region ($\alpha = 9,\ r = 12,\ \theta = 40^\circ$) and large loads $\Delta P_{L1} = \Delta P_{L2} = \Delta P_{L3} = 200$ MW 3–Areas/2–Block/Reduce–State/$\alpha = 9$.

trying more aggressive control objectives in order to "make the response faster", resulting thus in "high–gain" controllers laws which is well known that interact in a damaging way with the input saturators the presence of which has been neglected in the design phase.

The possibly detrimental interplay between "high–gain" control, and especially its integral action component, and saturation has recently become an important issue, since it has been shown that saturation induced oscillations or even instabilities can occur during the transient response as demonstrated in [13, 17, 18]. In [11] the same danger was shown to be in action in a single–area system when an aggressive control design addresses a power system with high load and an input saturator.

One way to handle this trade–off between performance and avoidance of triggering the saturation limits is via an appropriate ("ad hoc") selection of the LMI region (mainly its α and secondarily its r-parameter) so that the saturators work close to their limits (especially during the first seconds of the load variation) but without hitting their upper/lower (max or min) bounds. Even with a constant and known value on the expected load change $\Delta P_L(t)$, this implies a tedious search on the set of candidate LMI regions so that the saturated responses are only slightly overshooting when compared with their unsaturated versions [9, 11].

The primary cause of this perplexity being the designer's choice of LMI regions $D(\alpha, r, \theta)$ with large absolute values of parameter α (the minimum decay–rate) and large values of r (a constraint on the minimum damped frequency). Since our proposed approach relies on linear control tools, it is important to discuss this issue before the introduction of the AW scheme and offer some generic tuning guidelines extracted from extensive simulation results on the two–area benchmark system.

B. Demonstrating the need of "extra action" in case of Aggressive Control + Input Saturation + Large Loads

Since our proposed approach relies on linear control tools, it is important to discuss this issue before the introduction of the Gain 2-norm minimization and the Anti–Windup (AW) scheme and offer some tuning guidelines extracted from extensive simulation experiments on the two–area Model-2 benchmark system, delineating the concept of "control aggressivenes" and demonstrating the need for extra action (apart from H_∞ disturbance attenuation).

For the presentation in this (and the next) section the (amplitude) saturation is assumed to satisfy the following: (i) the control bounds $\Delta U^{tot}_{i,\max} \in \Re^*_+$ are equal and at least 10% larger than the maximum expected loads $\Delta P_{Li,\max}$ (i.e. $\Delta U^{tot}_{i,\max} = 220\ [MW]$ if $\Delta P_{Li,\max}$ is known to be 200MW), otherwise a zero frequency deviation would be simply unreachable. (ii)the saturator limits are "symmetric" in the sense that $\Delta U^{tot}_{i,\max} = -\Delta U^{tot}_{i,\min}$. Allowing negative values for $\Delta U^{tot}_{i,\min}$ is necessary in order to handle negative values of the ΔP_L components in case of load reduction.

The concept of "control aggressiveness" is quantified in Figure 13 depicting the family of curves for the ∞-norm of the gain vectors K_x, K_I and the corresponding attenuation level γ_∞ for increasing values of r and $\alpha = 1, 2, \ldots, 9$ when H_∞/Pole clustering control methodologies are used for a Model-2 two area example. The interpretation of the results in this Figure for design purposes is that **there exists a trade–off between two conflicting design objectives** since the desire for maximum disturbance attenuation (small values of γ_∞) is achieved with increasing values of r which, even with moderate values of the decay–rate parameter α, results in "large gains". This latter is against our desire to "keep the gains small" so that the saturators are not triggered. For our two areas simulations, a fixed choice of $r = 12$ was selected as a trade–off for the whole range of α's to be investigated in the nonlinear simulations below.

C. Enhancing the baseline H_∞/Pole Clustering LFC design with Gain 2-norm minimization: a multiobjective optimization setup

When input saturation is present, a crucial issue is that even if the set of H_∞/Pole Clustering LMIs (46) and (47) is feasible, the computed gains can become unacceptably "large" since no restrictions were formulated in the optimization procedure. It is well known that "large" gains interact harmfully with saturator nonlinearities since the resulting control signal $u(t) = Kx(t)$ does not necessarily respect the saturation limits [42, 43]. As shown in [14, 44] additional LMI constraints can be used on the separate matrices Y and X constituting the static state feedback gain $K = YX^{-1}$ in order to prevent the optimization procedure from producing "large gains". This is accomplished by observing that $\|Y\|_2$ can be bounded as

$$\begin{bmatrix} -\kappa_Y I_{Nx} & Y^T \\ Y & -I_{Nu} \end{bmatrix} < 0 \qquad (56)$$

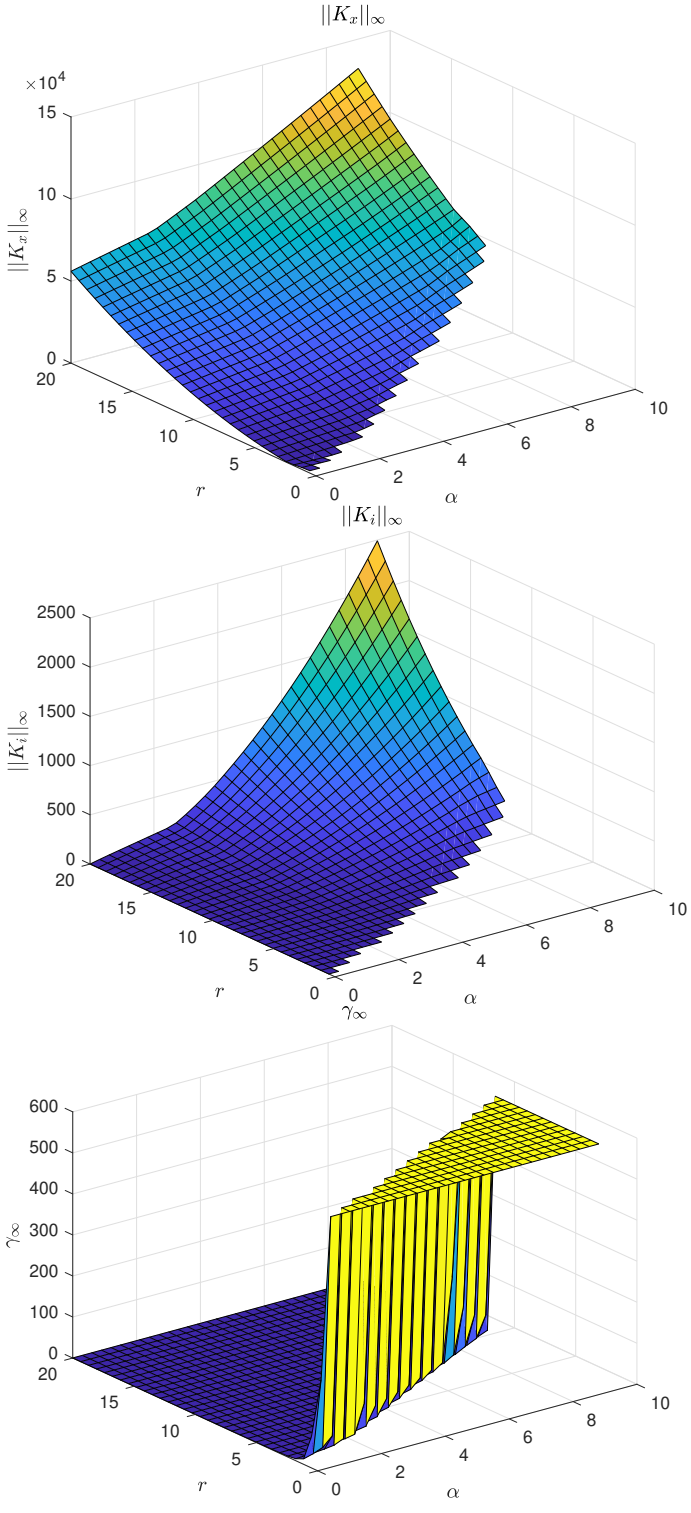

Fig. 13. $||K_x||_\infty$, $||K_i||_\infty$ vs. $\{\alpha,\ r\}$, $(\theta = 40^\circ)$

which, by Schur complement, is equivalent to $Y^TY < \kappa_Y I_{Nx}$ hence $\|Y\|_2 < \sqrt{\kappa_Y}$. In a similar manner, $\|X^{-1}\|_2$ can be bounded using the LMI constraint

$$\begin{bmatrix} X & I_{Nx} \\ I_{Nx} & \kappa_X I_{Nx} \end{bmatrix} > 0 \tag{57}$$

which, by Schur complement, is equivalent to $X^{-1} < \kappa_X I_{Nx}$ hence $\|X^{-1}\|_2 < \kappa_X$. Combining, it can be seen that the following norm bound can be achieved should the LMIs (56, 57) are feasible.

$$K^TK = X^{-1}Y^TYX^{-1} < \kappa_Y X^{-1}X^{-1} < \kappa_Y \kappa_X^2 I_{Nx}. \tag{58}$$

The LFC control design procedure can now be formulated as a multiobjective minimization problem for the augmented system (39), with the cost function being a weighted sum of the disturbance attenuation index γ and the norms of the X, Y matrices comprising the augmented state feedback gain $K = YX^{-1}$, subject to the LMI constraints expressing the requirements for disturbance rejection (H_∞), pole clustering and gain norm minimization.

Proposition 7: **minimize $\alpha_1\gamma + \alpha_2\kappa_X + \alpha_3\kappa_Y$ subject to the LMI constraints (46), (47), (56), (57).**

Remark 8: The controller gains, and the ensuing closed–loop responses, are sensitive to the values assigned on the weighting coefficients α_1, α_2, α_3, in Proposition 7 which are usually normalized so that

$$\sum_{i=1}^{3} \alpha_i = 1$$

. Hence it is important to discuss and offer some tuning guidelines for the choice of α_1, α_2, α_3. These guidelines, although reflecting the specific parameters of the LFC problem at hand, are summarized in the fact that **in the presence of input saturators it is always of higher importance to keep the gains "small" (large α_2 weight) even at the expense of disturbance attenuation (small α_1).**

For the benchmark two–areas example presented in section **??**, and all the simulation examples offered below, the controllers were computed with

$$\alpha_1 = 0.001,\ \alpha_2 = 0.998,\ \alpha_3 = \alpha_1 = 0.001 \tag{59}$$

reflecting the designer's choice of assigning higher importance on keeping the gains "small" even if the price to be paid is a deterioration of disturbance attenuation capacity, reflected in higher values of γ. This choice conforms with the heuristic rule provided in [44].

D. LMI based Linear Anti–Windup Enhancement

As shown in the previous section, it is possible that even in the case of or a simple two area electric power system, violent frequency and tie–line power oscillations can occur when input amplitude saturation co-exists with aggressive control designs and large loads. Similar results were provided even for an islanded area [11].

In order to improve the LFC controller capabilities and overcome the performance degradation arising from saturation, a linear anti-windup (AW) compensator will be designed and tuned. No rate constraints were taken into account although this could be a source of further complications [18, 42, 43, 45]. In [11], a Riccatti equation based approach presented in [45, 46] was adopted not only due to

its numerical advantage, but also because it provides the capability of tuning the dynamics of the AW compensator using a weighting matrix while preserving the L_2 performance.

In this work an LMI–based approach for the design of a full order AW compensator will be used, inspired by the methodology presented in chapter 5 of [47]. Figure 14 delineates the adapted architecture of the AW compensator to be designed.

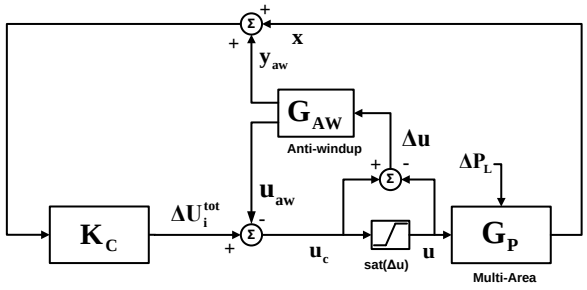

Fig. 14. Block-diagram of the proposed anti–windup scheme (inspired and adapted from [46, 47])

The block shown as G_p is the stable open–loop plant whose input is the total control signal ΔU^{tot} defined in (14) and having the state vector $y = x$ as measured output. The state space description of G_p

$$\begin{aligned} G_p \;:\; \dot{x}(t) &= A_{Np}x(t) + B_{uN}\Delta U^{tot}(t) + B_{wN}\Delta P_L(t), \\ y(t) &= x(t), \end{aligned} \tag{60}$$

has the same state vector and the same structure as that of S_o in (15), differing only in the system matrix A_{Np} which, in turn, is derived from A_N in (31) by neglecting the rows regarding the primary control action ("droop") embedded in the submatrix $A_t = \mathrm{diag}\big(K_{t1}/(R_1T_{t1}), \ldots, K_{tN}/(R_NT_{tN})\big)$. For our two areas example, matrix A_{2p} can be readily extracted from A_2, red in (52) as below:

$$A_{2p} = \begin{bmatrix} -\frac{1}{T_{p1}} & 0 & \frac{K_{p1}}{T_{p1}} & 0 & -\frac{K_{p1}}{T_{p1}} \\ 0 & -\frac{1}{T_{p2}} & 0 & \frac{K_{p2}}{T_{p2}} & \frac{K_{p2}}{T_{p2}} \\ 0 & 0 & -\frac{1}{T_{t1}} & 0 & 0 \\ 0 & 0 & 0 & -\frac{1}{T_{t2}} & 0 \\ K_{12} & -K_{12} & 0 & 0 & 0 \end{bmatrix} \tag{61}$$

For the special case of our N interconnected areas, being a strictly proper plant ($D_p = 0$) with unit output matrix $C_p = I$, the AW compensator of [47] can be cast in the following state space form:

$$G_{AW} : \begin{cases} \dot{x}_{aw}(t) = A_w x_{aw}(t) + B_p \Delta u(t) \\ u_{aw}(t) = F_w x_{aw}(t) \\ y_{aw}(t) = x_{aw}(t) \end{cases} \tag{62}$$

The matrix $A_w = A_{Np} + B_{uN}F_w$ is Hurwitz provided that the gain F_w has been properly designed, while u_{aw} and y_{aw} are the two outputs of the AW compensator, applied to the closed–loop system according to Figure 14. The role of the generated signal y_{aw} is to modify the measured output of the plant (the full state vector in our case), while u_{aw} is responsible for the modification of the control signal generated by the linear controller designed. The saturation block has the well known function

$$u(t) = \mathrm{sat}(u_c(t)) = \begin{cases} u_c(t) & \text{if } |u_c(t)| \le u_{\max} \\ u_{\max}\mathrm{sign}(u_c(t)) & \text{elsewhere} \end{cases} \tag{63}$$

and the term $\Delta u(t) = u_c(t) - u(t)$ (activated only when saturation occurs) is the saturation block input-output difference. According to [47] the suitable F_w is given by $F_w = LQ^{-1}$ if there are matrices $Q > 0 \in R^{n\times n}$, diagonal $U > 0 \in R^{n\times n}$, $L \in R^{m\times n}$ with n,m the number of states and inputs of G_p, and a positive real scalar γ_w such that the following LMI is feasible with respect to the decision variables $L,\ Q,\ U,\ \gamma_w$.

$$\begin{bmatrix} QA_p^T + A_pQ + & B_pU - L^T & 0 & QC_p^T + \\ L^TB_p^T + B_pL & & & L^TD_p^T \\ * & -2U & I & UD_p^T \\ * & * & -\gamma_w I & 0 \\ * & * & * & -\gamma_w I \end{bmatrix} < 0 \tag{64}$$

Remark 9: It should be emphasized that the ensuing AW compensator is independent of the LMI region chosen and the static feedback gains $K_x,\ K_i$ in (41) produced by the H_∞ and pole clustering LMIs.

Moreover, the selected anti–windup scheme belongs to the family of "model recovery" algorithms [42, 43] which, in the presence of saturators, try to recover the response of the stable open–loop linear system in (60). Hence the transient performance of the closed–loop system with saturation and anti–windup cannot be faster than that of (60), often resulting in a rather sluggish response when loads are smaller than the nominal ones.

E. Demonstration of the Windup Problem and its AW solution

Due to space limitations only one example will be given for the windup problem and the proposed solutions. The example uses the two area benchmark example of section III-C.2 and the aggressiveness is expressed by demanding pole clustering in the LMI region ($\alpha = 9,\ r = 12,\ \theta = 40^\circ$). The baseline controller is designed using the H_∞, pole clustering and gain norm minimization LMIs and tuned for the nominal loads. The integrator windup problem shows up and a linear anti–windup compensator is added to handle the windup problem. Although this seems to be an "academic example", it is a valid demonstration of the windup issues arising when what we call "a purely linear mentality ignoring input saturation" is employed.

The control synthesis problem when the gain 2-norm restrictions expressed via the LMIs (56),(57) are taken into account was formulated and solved as a multiobjective minimization problem with the weighting factors presented in (59) i.e. $\alpha_1 = 0.001,\ \alpha_2 = 0.998,\ \alpha_3 = \alpha_1 = 0.001$. The state–feedback and integral gains, the disturbance attenuation γ and the closed–loop eigenvalues achieved are

$$K_x = 10^4 \begin{bmatrix} -5.2190 & 1.4582 & -0.0009 & 0.0001 & 0.0059 \\ 1.4581 & -5.2190 & 0.0001 & -0.0009 & -0.0059 \end{bmatrix}$$

$$K_I = \begin{bmatrix} -461.0555 & 271.5807 \\ 271.5801 & -461.0560 \end{bmatrix}$$

with a guaranteed disturbance attenuation of $\gamma = 117.7577$. The achieved closed–loop eigenvalues are

$$-9.3736 \pm 6.8341i, \quad -9.2079 \pm 3.1225i$$
$$-9.0955 \pm 7.6209i, \quad -9.9733$$

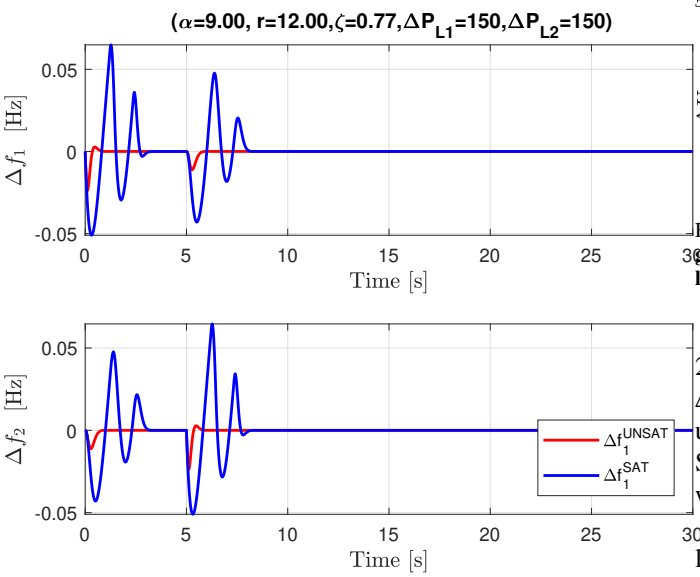

Fig. 15. $\Delta f_{1,2}(t)$ responses **with 2-norm gain restriction** for the aggressive LMI region ($\alpha = 9,\ r = 12$), **and nominal loads** $\Delta P_{L1} = \Delta P_{L2} = +150$ MW.

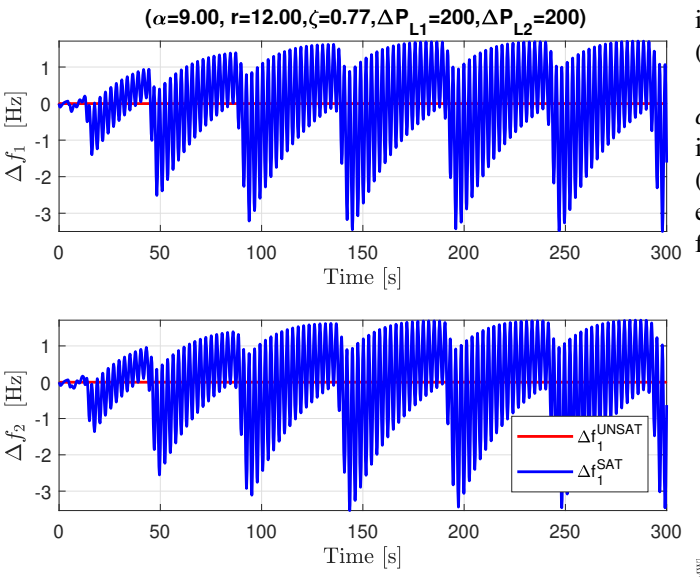

Fig. 16. $\Delta f_{1,2}(t)$ responses **with 2-norm gain restriction** for the aggressive LMI region ($\alpha = 9,\ r = 12$), **and large loads** $\Delta P_{L1} = \Delta P_{L2} = +200$ MW.

1) LMI Region9 - System responses with nominal Loads and large loads - no AW : Despite the excessive aggressiveness of the chosen LMI region, the controller tuning with

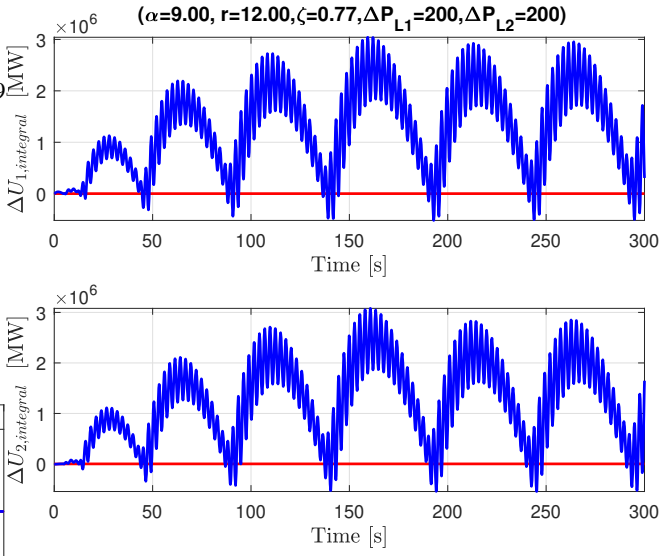

Fig. 17. The Integral Action component of the control signal **with 2-norm gain restriction** for the aggressive LMI region ($\alpha = 9,\ r = 12$), **and large loads** $\Delta P_{L1} = \Delta P_{L2} = +200$ MW.

2-norm gain restriction proves adequate for nominal loads $\Delta P_{L1} = \Delta P_{L2} = +150$ MW as depicted in Figure 15 with the unsaturated (red) and the saturated (blue) system responses. Similar responses (with larger settling times) were derived without 2-norm gain restriction and nominal loads.

Figure 16 presents the same responses (300 seconds) with large loads $\Delta P_{L1} = \Delta P_{L2} = +200$ MW. In this case it is clear that the 2-norm gain minimization is not an adequate cure for the windup problem manifested as violent frequency (and tie–line power) oscillations. Figure 17 depicts the root cause of the violent oscillations in the saturated responses in Figure 16 which is the "Integrator windup" due to "large (integral) gains".

2) LMI Region9 - System responses with large loads and centralized (multivariable) AW compensator: A fully centralized Linear AW compensator whose structure is presented in (62), is designed with the LMI tools presented in (64)), and employed in this demanding situation of an aggressive choice for LMI region combined with larger–than–nominal loads.

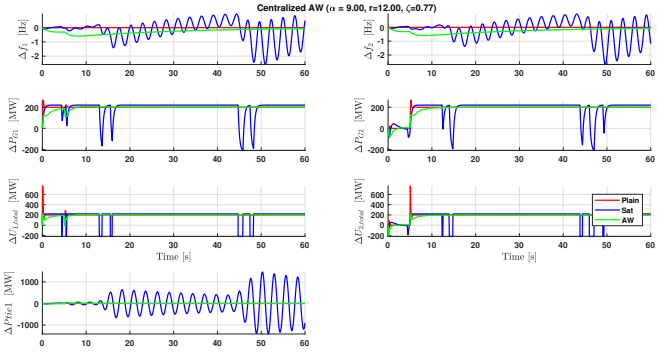

Fig. 18. All system responses with a fully centralized AW (**with 2-norm gain restriction**) for the aggressive LMI region ($\alpha = 9,\ r = 12$) and large loads $\Delta P_{L1} = \Delta P_{L2} = 200\ MW$.

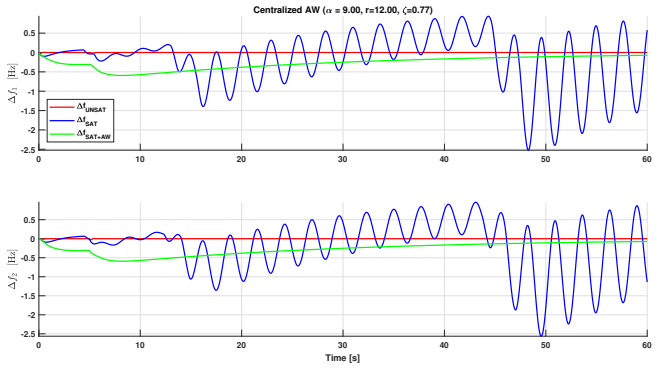

Fig. 19. $\Delta f_{1,2}(t)$ responses with a fully centralized AW (**with 2-norm gain restriction**) for the aggressive LMI region ($\alpha = 9,\ r = 12$) and large loads $\Delta P_{L1} = \Delta P_{L2} = 200\ MW$.

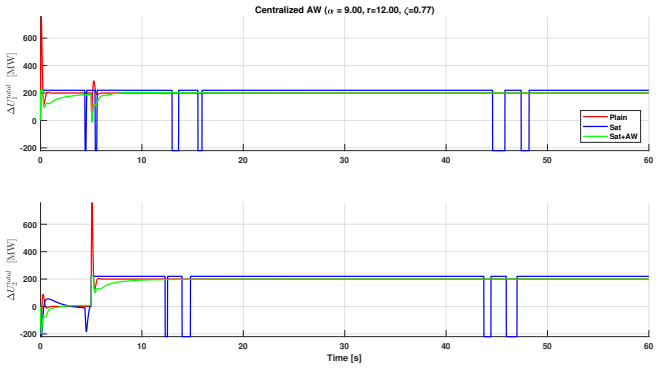

Fig. 20. $\Delta U^{tot}_{1,2}(t)$ responses with a fully centralized AW (**with 2-norm gain restriction**) for the aggressive LMI region ($\alpha = 9,\ r = 12$) and large loads $\Delta P_{L1} = \Delta P_{L2} = 200\ MW$.

It should be emphasized that this scheme **not only guarantees the stability of the composite closed–loop system (with the saturators included) but also suppresses the violent frequency and tie–line oscillations even if the 2-norm gain minimization restriction is not used** as can be seen in Figure18, depicting all system responses from both areas, with the fully centralized (multivariable) AW in place and the Linear Controller designed **with the 2-norm gain restriction**.

Figures 19 and 20 present a closer look at the frequency and the total control action. As can be seen the ensuing AW compensator, trying to "recover" the response of the stable open–loop system in (60) suppresses the violent oscillations, acting as a low–pass filter.

V. Conclusions

This research work addressed two objectives: (i) linear analysis and (ii) linear control design for the Load Frequency Control problem for electric power systems consisting of multiple interconnected power areas taking into account input saturation.

Starting with a systematic presentation of three modelling approaches of increasing complexity for the linearized versions of LFC, the main contribution in the linear analysis is the proof that there exists an inherent controllability problem (an uncontrollable pole at the origin/non–minimal realization). The reason for this "controllability loss" is the graph Laplacian which reflects the structure of the reactive interconnecting tie–lines. Analysis continues by proving that due to the specific properties of the graph Laplacian it is possible to "single out" and discard the redundant state variable acquiring a controllable reduced state model.

Mature LMI–based H_∞ control methodologies are then used for centralized linear control design and tuning, based on both the full–state (uncontrollable) models and the reduced–state (controllable) models.

The controllable (reduced state) models give the chance to investigate the interaction of the proposed linear controllers with input saturators modelling the hard constraints on the speed governor and the steam servo–valves. Controllers of increasing aggressiveness are shown to interact in a detrimental way with the saturation nonlinearity even in the case of two–area benchmark systems especially in the case of larger–than–nominal loads hit the network. Two linear schemes are then proposed as enhancements to the as a solution (i) minimization of the 2-norm of the controller gains (ii) a linear anti–windup compensator which guarantees closed–loop stability and at the same time filters the violent frequency and tie–line power oscillations that possibly manifest in case of large loads. These remedies though come at a price: the sluggishness of the closed–loop responses when the loads are smaller than nominal. Extensive simulation studies on two-area and three areas benchmark power systems highlight the efficiency of the proposed modelling and control schemes.

Directions for future work include (i) robustness analysis with respect to measurement delays and parametric uncertainties in the models - design of LFC (ii) making the proposed controllers distributed and/or decentralized (iii)the investigation of recent results in the anti–windup schemes that are not bound to the "model recovery approach".

Appendix

A. 3–Areas,3–Block,Full–State–Vector: LFC using Decentralized Purely Integral Control (Nominal + Uncertain)

The three equal loads $\Delta P_{Li} = 200$MW hit the three areas at $t = 1, 5, 9$s respectively.

Figure 21 shows the system responses with Decentralized Purely Integral Control. The three (equal) gains were tuned by trial and error and finally set into $K_i = -0.4$. Settling time is approximately 25 seconds.

Keeping the same Integral Gain ($K_i = -0.4$) the actual system parameters K_{pi}/T_{pi} are now perturbed (increased/decreased) by 40% respectively, that is $K_{pi}^{actual} = 1.40 \times K_{pi}^{nominalal}$ and $T_{pi}^{actual} = 0.60 \times T_{pi}^{nominal}$. This drastic parameter perturbation affects the matrix B_f. Figure 22 shows the deteriorated system responses. Settling time is now approximately 60 seconds.

Figure 23 shows the unstable system responses with K_{pi}/T_{pi} parameters perturbed (increased/decreased) by 50% respectively, that is $K_{pi}^{actual} = 1.50 \times K_{pi}^{nominal}$ and $T_{pi}^{actual} = 0.50 \times T_{pi}^{nominal}$.

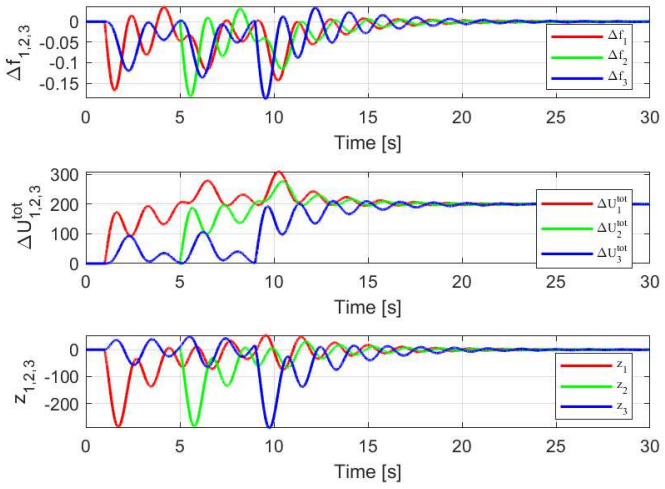

Fig. 21. $\Delta f_{1,2,3}(t)$, $z_{1,2,3}(t)$ responses with Decentralized Purely Integral Control and large loads $\Delta P_{L1} = \Delta P_{L2} = \Delta P_{L3} = 200$ MW and $K_i = -0.4$. 3–Areas/3–Block/Full–State/$K_i = -0.4$.

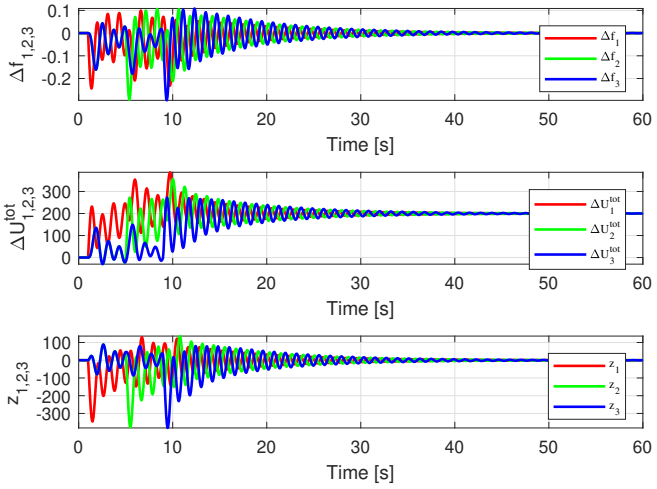

Fig. 22. $\Delta f_{1,2,3}(t)$, $z_{1,2,3}(t)$ responses with Decentralized Purely Integral Control, uncertain K_{pi}, T_{pi} parameters and large loads $\Delta P_{L1} = \Delta P_{L2} = \Delta P_{L3} = 200$ MW and $K_i = -0.4$. 3–Areas/3–Block/Full–State/Uncertain/$K_i = -0.4$/and $\pm 40\%$ uncertainty in K_{pi}, T_{pi} .

B. 3–Areas,3–Block,Full–State–Vector: LFC using H_∞/Pole Clustering (Nominal + Uncertain)

Figure 24 shows the frequency deviations $\Delta f_{1,2,3}(t)$, the total control action $\Delta U^{tot}_{1,2,3}(t)$ and the performance variables ("ACEs") $z_{1,2,3}(t)$ of Area1,Area2 and Area3 with H_∞ control and pole clustering inside the convex LMI region with $\alpha = 0$ and $r = 12$, $\theta = 40°$. The achieved attenuation was $\gamma_{opt} = 18.2321$. The settling time is within prescribed limits and the steady state errors are zero. The $12+3 = 15$ closed–loop eigenvalues, with their real parts being less or equal to 0 as prescribed, are now

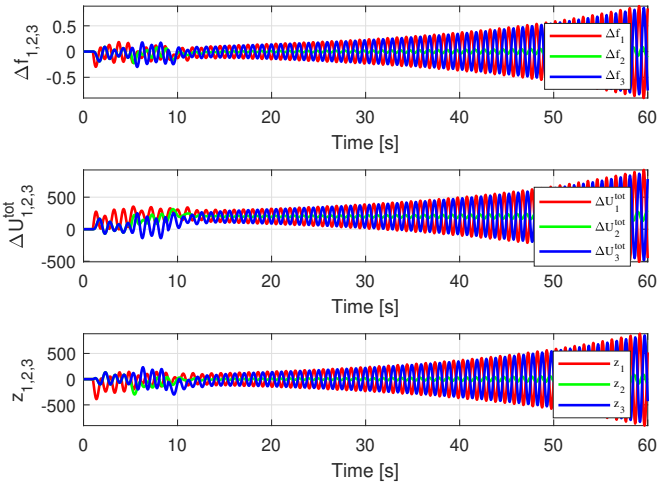

Fig. 23. $\Delta f_{1,2,3}(t)$, $z_{1,2,3}(t)$ responses with Decentralized Purely Integral Control, uncertain K_{pi}, T_{pi} parameters and large loads $\Delta P_{L1} = \Delta P_{L2} = \Delta P_{L3} = 200$ MW and $K_i = -0.4$. 3–Areas/3–Block/Full–State/Uncertain/$K_i = -0.4$/and $\pm 50\%$ uncertainty in K_{pi}, T_{pi} .

$$-6.5527 \pm 2.7619i,\ -6.5195 \pm 2.6585i,\ -5.6008 \pm 0.1965i$$
$$-2.2912,\ -2.0450 \pm 0.4203i,\ -1.8754,$$
$$-1.2006,\ -0.5235,\ -0.2653,\ -0.2614,\ 0.000$$

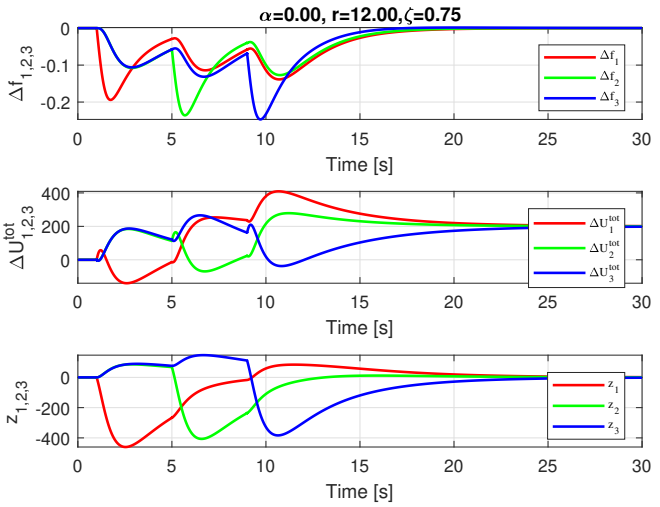

Fig. 24. $\Delta f_{1,2,3}(t)$, $\Delta U^{tot}_{1,2,3}(t)$ and $z_{1,2,3}(t)$ responses with H_∞ control and Pole Clustering within the LMI region ($\alpha = 0$, $r = 12$, $\theta = 40°$ and large loads $\Delta P_{L1} = \Delta P_{L2} = \Delta P_{L3} = 200$ MW 3–Areas/3–Block/Full–State/HinfDstab .

Keeping the same H_∞+Pole–clustering objectives, and computing the gains based on the nominal values of the system parameters, we now perturb the actual system parameters K_{pi}/T_{pi} (increased K_{pi}/decreased T_{pi} by the same amount). Figure 25 shows the slightly deteriorated system responses with a 50% perturbation, affecting the matrix B_f, that is $K_{pi}^{actual} = 1.50 \times K_{pi}^{nominalal}$ and $T_{pi}^{actual} = 0.50 \times T_{pi}^{nominal}$. Both the frequencies and the ACEs converge to zero in approximately 25 seconds. Figure 26 shows the deteriorated system responses with a drastic 75% perturbation,affecting

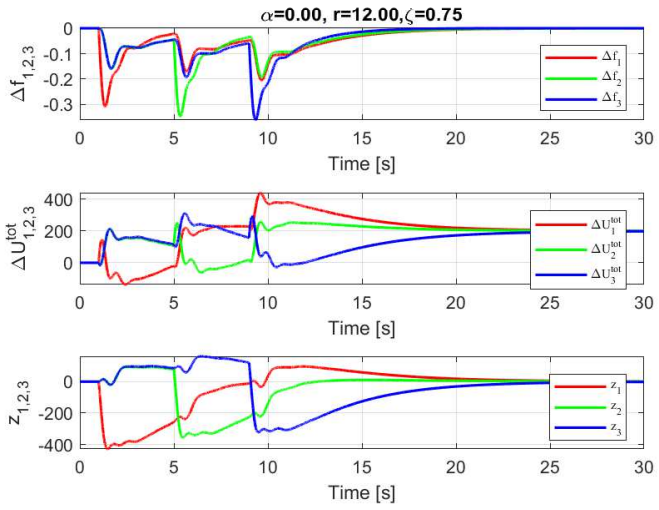

Fig. 25. $\Delta f_{1,2,3}(t)$, $\Delta U^{tot}_{1,2,3}(t)$ and $z_{1,2,3}(t)$ responses with H_∞ control and Pole Clustering within the LMI region $\alpha = 0$, $r = 12$, $\theta = 40°$, and large loads $\Delta P_{L1} = \Delta P_{L2} = \Delta P_{L3} = 200$ MW 3–Areas/3–Block/Full–State/Uncertain/HinfDstab, ±50% uncertainty in K_{pi}, T_{pi} .

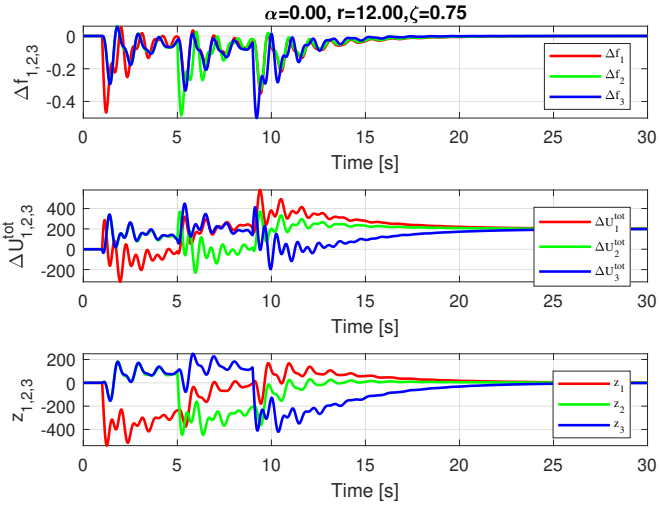

Fig. 26. $\Delta f_{1,2,3}(t)$, $\Delta U^{tot}_{1,2,3}(t)$ and $z_{1,2,3}(t)$ responses with H_∞ control and Pole Clustering within the LMI region $\alpha = 0$, $r = 12$, $\theta = 40°$, and large loads $\Delta P_{L1} = \Delta P_{L2} = \Delta P_{L3} = 200$ MW 3–Areas/3–Block/Full–State/Uncertain/HinfDstab, ±75% uncertainty in K_{pi}, T_{pi} .

the matrix B_f, that is $K_{pi}^{actual} = 1.75 \times K_{pi}^{nominal}$ and $T_{pi}^{actual} = 0.25 \times T_{pi}^{nominal}$. Again both the frequencies and the ACEs converge to zero in approximately 25 seconds.

C. 4–Areas,3–Block,Full–State–Vector: LFC using Decentralized Purely Integral Control (Nominal + Uncertain)

Figure 27 shows the system responses with Decentralized Purely Integral Control. The three (equal) gains were tuned by trial and error and finally set into $K_i = -0.3$. Settling time is approximately 25 seconds.

Keeping the same Integral Gain ($K_i = -0.3$) the actual system parameters K_{pi}/T_{pi} are now perturbed (increased/decreased) by 30% respectively, that is $K_{pi}^{actual} = 1.30 \times K_{pi}^{nominalal}$ and $T_{pi}^{actual} = 0.70 \times T_{pi}^{nominal}$. This drastic parameter perturbation affects the matrix B_f. Figure 28 shows the deteriorated system responses. Settling time is clearly beyond 30 seconds.

Figure 29 shows the unstable system responses with K_{pi}/T_{pi} parameters perturbed (increased/decreased) by 50% respectively, that is $K_{pi}^{actual} = 1.50 \times K_{pi}^{nominal}$ and $T_{pi}^{actual} = 0.50 \times T_{pi}^{nominal}$.

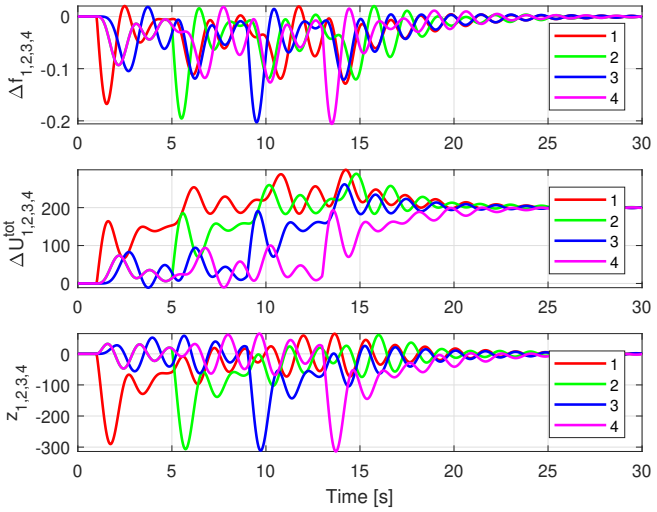

Fig. 27. $\Delta f_{1,2,3,4}(t)$, $z_{1,2,3,4}(t)$ responses with Decentralized Purely Integral Control, Nominal Design and large loads $\Delta P_{Li} = 200$ MW and $K_i = -0.3$. 4–Areas/3–Block/Full–State/$K_i = -0.3$/Nominal Design .

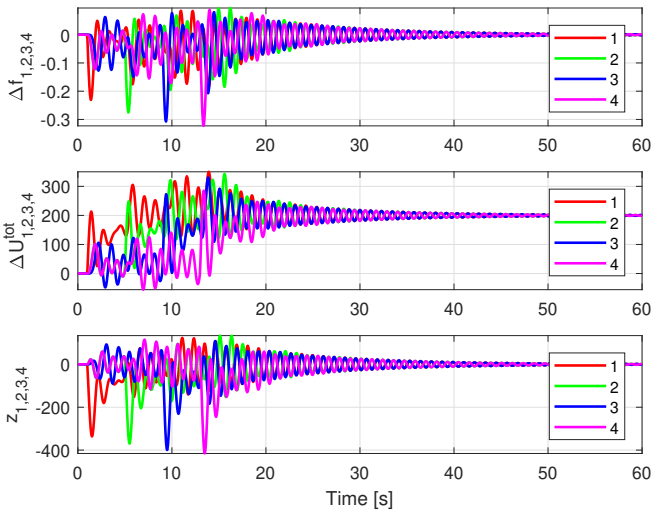

Fig. 28. $\Delta f_{1,2,3,4}(t)$, $z_{1,2,3,4}(t)$ responses with Decentralized Purely Integral Control, uncertain K_{pi}, T_{pi} parameters large loads $\Delta P_{Li} = 200$ MW and $K_i = -0.3$. 4–Areas/3–Block/Full–State/$K_i = -0.3$, ±30% uncertainty in K_{pi}, T_{pi} .

D. 4–Areas,3–Block,Full–State–Vector: LFC using H_∞/Pole Clustering (Nominal + Uncertain)

Note that the H_∞ LMIs were infeasible for $\theta = 40°$ had to increase into $\theta = 45°$.

Figure 30 shows the frequency deviations $\Delta f_{1,2,3,4}(t)$, the total control action $\Delta U^{tot}_{1,2,3,4}(t)$ and the performance variables

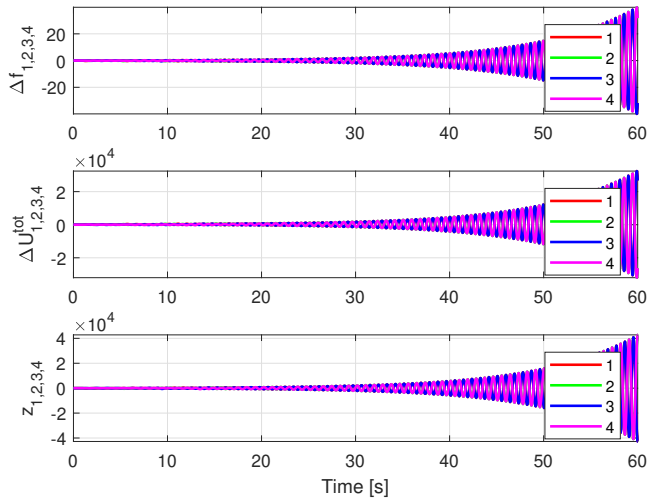

Fig. 29. $\Delta f_{1,2,3,4}(t)$, $z_{1,2,3,4}(t)$ responses with Decentralized Purely Integral Control, uncertain K_{pi}, T_{pi} parameters large loads $\Delta P_{Li} = 200$ MW and $K_i = -0.3$. 4–Areas/3–Block/Full–State/$K_i = -0.3$, $\pm 50\%$ uncertainty in K_{pi}, T_{pi} .

("ACEs") $z_{1,2,3,4}(t)$ of Area1,Area2,Area3 and Area4 with H_∞ control and pole clustering inside the convex LMI region with $\alpha = 0$ and $r = 12$, $\theta = 45°$. The achieved attenuation was $\gamma_{opt} = 35.2942$. Settling time is within prescribed limits -approximately 25 seconds- and the steady state errors are zero .

Figure 31 shows the deteriorated system responses with a drastic 75% perturbation, affecting the matrix B_f, that is $K_{pi}^{actual} = 1.75 \times K_{pi}^{nominal}$ and $T_{pi}^{actual} = 0.25 \times T_{pi}^{nominal}$. Both the frequencies and the ACEs converge to zero in approximately 30 seconds.

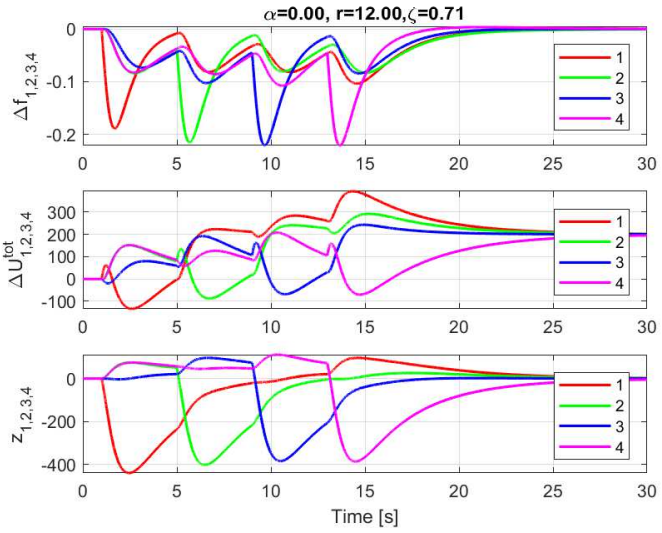

Fig. 30. $\Delta f_{1,2,3,4}(t)$, $\Delta U^{tot}_{1,2,3,4}(t)$ and $z_{1,2,3,4}(t)$ responses with H_∞ control and Pole Clustering within the LMI region ($\alpha = 0$, $r = 12$, $\theta = 45°$ and large loads $\Delta P_{L1} = \Delta P_{L2} = \Delta P_{L3} = 200$ MW 4–Areas/3–Block/Full–State/HinfDstab .

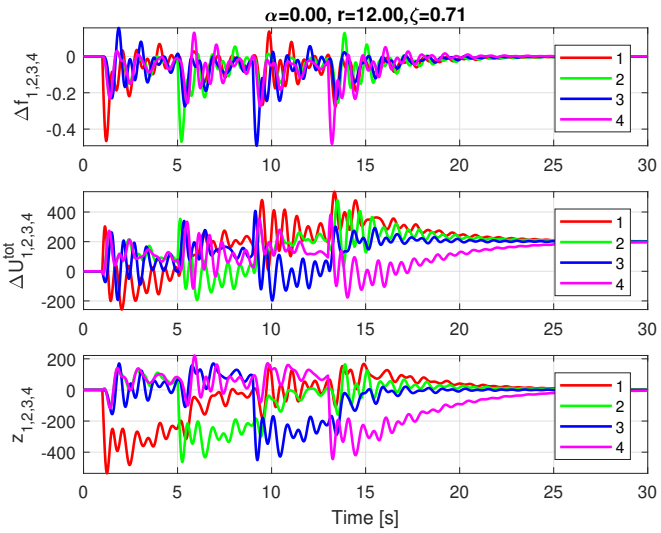

Fig. 31. $\Delta f_{1,2,3,4}(t)$, $\Delta U^{tot}_{1,2,3,4}(t)$ and $z_{1,2,3,4}(t)$ responses with H_∞ control and Pole Clustering within the LMI region ($\alpha = 0$, $r = 12$, $\theta = 45°$, uncertain K_{pi}, T_{pi} parameters and large loads $\Delta P_{L1} = \Delta P_{L2} = \Delta P_{L3} = 200$ MW 4–Areas/3–Block/Full–State/HinfDstab, $\pm 75\%$ uncertainty in K_{pi}, T_{pi} .

ACKNOWLEDGMENTS

Leonidas Dritsas acknowledges financial support from the Special Account for Research of ASPETE through the funding program "Strengthening research of ASPETE faculty members"

REFERENCES

[1] O. Elgerd, *Electric energy systems theory: an introduction*. McGraw-Hill, 1982.

[2] P. Kundur, *Power System Stability and Control*. McGraw-Hill, 1994.

[3] H. Bevrani, *Robust Power System Frequency Control (2nd Ed.)*. Springer, 2014.

[4] A. Bidram, F. Lewis, and A. Davoudi, "Distributed Control Systems for Small-Scale Power Networks: Using Multiagent Cooperative Control Theory," *IEEE Control Systems Magazine*, vol. 34, pp. 56–77, December 2014.

[5] E. Kontouras, A. Tzes, and L. Dritsas, "Covert attack on a discrete-time system with limited use of the available disruption resources," in *Proc. of the 2015 European Control Conference*, pp. 806–811, 2015.

[6] E. Kontouras, A. Tzes, and L. Dritsas, "Adversarial control scheme for an islanded power plant," in *Proc. of the 2016 European Control Conference*, (Aalborg, Denmark, June 29 - July 1), pp. 307–312, 2016.

[7] E. Kontouras, A. Tzes, and L. Dritsas, "Impact Analysis of a Bias Injection Cyber-Attack on a Power Plant," in *Proc. of the 20th IFAC World Congress*, (Toulouse, France, July 9-14), pp. 11586–11591, 2017.

[8] E. Kontouras, A. Tzes, and L. Dritsas, "Cyber-Attack on a Power Plant using Bias Injected Measurements," in *Proc. of the 2017 American Control Conference*, (Seattle, USA, May 24-26), pp. 5507–5512, 2017.

[9] L. Dritsas, E. Kontouras, I. Kitsios, and A. Tzes, "Load Frequency Control for Demand Disturbance Attenuation and Transient Response Improvement for a Single-Area Power Plant," in *Proc. of the 25th Mediterranean Conference on Control and Automation*, (Valletta, Malta, July 3-6), pp. 502–507, 2017.

[10] E. Kontouras, A. Tzes, and L. Dritsas, "Set-Theoretic Detection of Bias Injection Cyber-Attacks on Networked Power Systems," in *Proc. of the 2018 American Control Conference*, (Milwaukee, USA, June 27-29), pp. 5507–5512, 2018.

[11] L. Dritsas, E. Kontouras, I. Kitsios, and A. Tzes, "Aggressive Control Design for Electric Power Generation Plants," in *Proc. of the 26th Mediterranean Conference on Control and Automation*, (Zadar, Croatia, June 19-22), pp. 667–672, 2018.

[12] E. Kontouras, A. Tzes, and L. Dritsas, "Set-theoretic detection of data corruption attacks on cyber physical power systems," *J. Mod. Power Syst. Clean Energy*, vol. 6, pp. 872–886, September 2018.

[13] P. Esfahani, M. Vrakopoulou, K. Margellos, J. Lygeros, and G. Andersson, "Cyber attack in a two area power system: Impact identification using reachability," in *Proc. of the American Control Conference*, pp. 962–967, 2010.

[14] D. Siljak, D. Stipanovic, and A. Zecevic, "Robust Decentralized Turbine/Governor Control Using Linear Matrix Inequalities," *IEEE Transactions on Power Systems*, vol. 17, no. 3, pp. 715–722, 2002.

[15] H. Shayeghi, "A robust decentralized power system load frequency control," *Journal of Electrical Engineering*, vol. 59, no. 6, pp. 281–293, 2008.

[16] S. M. Tabatabaeipour, "Optimal Decentralized Control of Power Systems with Guaranteed Damping," in *Proc. of the European Control Conference*, pp. 223–228, 2015.

[17] J. Liu, B. Krogh, and M. Ilic, "Saturation-induced Instability in electric power systems," in *Proc. of the American Control Conference*, pp. 580–585, 2008.

[18] C. Huang, D. Yue, and X. Xie, "Anti-Windup Load Frequency Controller Design for Multi-Area Power System with Generation Rate Constraint," *Energies*, vol. 9, no. 5, 2016.

[19] B. Pal and B. Chaudhuri, *Robust Control in Power Systems*. Springer, 2005.

[20] A. Bidram, V. Nasirian, A. Davoudi, and F. Lewis, *Cooperative Synchronization in Distributed Microgrid Control*. Springer, 2017.

[21] J. Ma, *Power System Wide-area Stability Analysis and Control*. Wiley, 2018.

[22] H. Shayeghi, H. Shayanfar, and A. Jalili, "Load frequency control strategies: A state-of-the-art survey for the researcher," *Energy Conversion and Management*, vol. 50, no. 2, pp. 344 – 353, 2009.

[23] S. Pandey, S. Mohanty, and N. Kishor, "A literature survey on load frequency control for conventional and distribution generation power systems," *Renewable and Sustainable Energy Reviews*, vol. 25, pp. 318 – 334, 2013.

[24] R. Shankar, S. Pradhan, K. Chatterjee, and R. Mandal, "A comprehensive state of the art literature survey on LFC mechanism for power system,"

[25] M. Brinda, A. Suresh, and M. Rashmi, "A literature survey on lfc in a deregulated electricity environment," *World Review of Science, Technology and Sust. Development*.

[26] H. Alhelou, M. Hamedani, R. Zamani, E. Forushani, and P. Siano, "Challenges and opportunities of load frequency control in conventional, modern and future smart power systems: A comprehensive review," *Energies*, vol. 9, September 2018.

[27] X. Yu and K. Tomsovic, "Application of linear matrix inequalities for load frequency control with communication delays," *IEEE Transactions on Power Systems*, vol. 19, pp. 1508–1515, 2004.

[28] K. Tomsovic, D. Bakken, V. Venkatasubramanian, and A. Bose, "Designing the next generation of real-time control, communication, and computations for large power systems," *Proceedings of the IEEE*, vol. 93, pp. 965–979, 2005.

[29] A. Kanchanaharuthai and P. Ngamsom, "Robust hinf load-frequency control for interconnected power systems with d-stability constraints via lmi approach," in *Proc. of the 2015 American Control Conference*, (Portland, OR, USA, June 8-210), pp. 4387–4392, 2005.

[30] K. S. Parma, S. Majhi, and D. Kothari, "Load frequency control of a realistic power system with multi-source power generation," *International Journal of Electrical Power & Energy Systems*, vol. 42, pp. 426–433, November 2012.

[31] M. Mesbahi and M. Egerstedt, *Graph theoretic methods in multiagent networks*. Princeton University Press, 2010.

[32] B. Mohar, "The Laplacian spectrum of graphs," *Graph theory Comb. Appl.*, 1991.

[33] M. Andreasson, D. Dimarogonas, H. Sandberg, and K. Johansson, "Distributed Control of Networked Dynamical Systems: Static Feedback, Integral Action and Consensus," *IEEE Transactions on Automatic Control*, vol. 59, pp. 1750–1764, July 2014.

[34] M. Andreasson, D. Dimarogonas, H. Sandberg, and K. Johansson, "Distributed PI-control with applications to power systems frequency control," in *Proc. of the American Control Conference*, pp. 3183–3188, 2014.

[35] M. Andreasson, D. Dimarogonas, K. Johansson, and H. Sandberg, "Distributed vs. centralized power systems frequency control under unknown load changes," in *Proc. of the European Control Conference*, pp. 3524–3529, 2013.

[36] C. Bechlioulis, L. Dritsas, and K. Kyriakopoulos, "Decentralized Load Frequency Control with Prescribed Performance for Interconnected Power Systems," in *submitted to 2019 IEEE Conference on Decision and Control (CDC)*, 2019.

[37] E. Vlahakis, L. Dritsas, and G. Halikias, "Distributed lqr design for identical dynamically coupled systems: Application to load frequency control of multi-area power grid," in *submitted to 2019 IEEE Conference on Decision and Control (CDC)*, 2019.

[38] P. Young and J. Willems, "An approach to the linear multivariable servomechanism problem," *International Journal of Control*, vol. 15, pp. 961–979, May 1972.

[39] E. Lavretsky and K. Wise, *Robust and Adaptive Control With Aerospace Applications*. Springer, 2013.

[40] P. Gahinet and P. Apkarian, "A linear matrix inequality approach to H_∞ control," *International journal of robust and nonlinear control*, vol. 4, no. 4, 1994.

[41] M. Chilali and P. Gahinet, "H_∞ Design with Pole Placement Constraints: An LMI Approach," *IEEE Transactions on Automatic Control*, vol. 41, pp. 358–367, Mar. 1996.

[42] S. Tarbouriech, G. G. G. da Silva, and J. Queinnec, *Stability and Stabilization of Linear Systems with Saturating Actuators*. Springer, 2011.

[43] L. Zaccarian and A.Teel, *Modern Anti-windup Synthesis: Control Augmentation for Actuator Saturation*. Princeton University Press, 2011.

[44] A. Zecevic and D. Siljak, *Control of Complex Systems: Structural Constraints and Uncertainty*. Springer, 2010.

[45] J. Sofrony, M. Turner, and I. Postlethwaite, "Anti-windup synthesis for systems with rate-limits using Riccati equations ," *International Journal of Control*, vol. 83, no. 2, 2010.

[46] J. Sofrony, M. Turner, and I. Postlethwaite, "Anti-windup synthesis using Riccati equations ," *International Journal of Control*, vol. 80, no. 1, pp. 112–128, 2007.

[47] M. Turner and D. Bates, *Mathematical Methods for Robust and Nonlinear Control*, vol. 367, 2007. Springer-Verlag London.